Development of nanoparticle thermosensor for microthermography in small living animals

Ferdinandus

2016

Ferdinandus. (2016). Development of nanoparticle thermosensor for microthermography in small living animals. Master's thesis, Nanyang Technological University, Singapore.

https://hdl.handle.net/10356/69013

https://doi.org/10.32657/10356/69013

DEVELOPMENT OF NANOPARTICLE THERMOSENSOR FOR MICROTHERMOGRAPHY IN SMALL LIVING ANIMALS

FERDINANDUS

2016

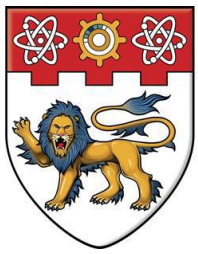

NANYANG TECHNOLOGICAL UNIVERSITY

DEVELOPMENT OF NANOPARTICLE THERMOSENSOR FOR MICROTHERMOGRAPHY IN SMALL LIVING ANIMALS

FERDINANDUS

SCHOOL OF MECHANICAL AND AEROSPACE ENGINEERING

NANYANG TECHNOLOGICAL UNIVERSITY

2016

DEVELOPMENT OF NANOPARTICLE THERMOSENSOR FOR MICROTHERMOGRAPHY IN SMALL LIVING ANIMALS

FERDINANDUS

FERDINANDUS

School of Mechanical and Aerospace Engineering

A thesis submitted to the Nanyang Technological University

in partial fulfillment of the requirements for the degree of

Master of Engineering

2016

Abstract

Insects produce heat through various muscular activities in order to maintain their body temperature balance with the surrounding environment through a process known as thermogenesis. In most endothermic flying insects, heat is majorly produced internally at their flight muscles. Therefore, obtaining temperature information from these activities at the microscale could give a valuable insight about the physiological function and behaviour in insects and other small animals. Although recent developments in electronic devices enable temperature sensors to work at high spatial resolution, their application for *in vivo* thermography is limited. For instance, infrared thermography (IRT), a commonly used tool for thermographic study in animals, is unable to detect the temperature distribution in small animals without specially designed lens. Thermal-dependent luminescence materials, on the other hand, have been developed in the past decade and frequently utilized for *in vivo* temperature sensing with high spatial resolution up to the nanoscale.

In this project, luminescence ratiometric nanoparticle thermosensors (RNTs) were prepared to map out the temperature distribution in small animals. Two different RNTs were fabricated employing the facile nano-precipitation process in which a temperature sensitive dye and a less temperature sensitive dye as a reference were embedded together in a polymer matrix. Ratiometric analysis was carried out by measuring the intensity of the temperature sensitive dye relative to that of the reference in order to negate the change in luminescence intensity owing to the

uneven sensor distribution or the z-axis sample displacement. The RNTs were then loaded into the subject animals to map out and monitor the temperature distribution within the target organelles of the animal.

The first type of RNT consists of EuDT as the temperature sensitive dye and $Ir(ppy)_3$ as the reference. Screening was performed by preparing RNTs with different polymer matrixes to investigate their stability in the solution form and their *in vitro* temperature sensitivity. The RNTs were then orally dosed into *D. melanogaster* larvae to demonstrate the *in vivo* thermography. The RNTs displayed a high *in vitro* sensitivity and were able to map out the *in vivo* temperature distribution in the larvae.

The second type of RNT encompasses EuDT and rhodamine 800 as the reference, both embedded in PS-MA matrix. The RNT was loaded into *D. derbyana* flight muscle in order to monitor and map out the temperature change during the pre-flight preparation process in the beetle. This type RNT allows direct use of the luminescence intensity of the dyes for *in vivo* ratiometric intensity analysis owing to the low autofluorescence signal contribution from the muscle. High spatial resolution temperature monitoring and mapping were achieved in detecting the physiological heat production and transfer in the flight muscle of the beetle.

Both the RNTs prepared exhibit high *in vitro* and *in vivo* temperature sensitivity with fairly good temperature resolution. Moreover, the RNTs efficiently worked in detecting the temperature shift in small living animals *in vivo*, either due to an external heat source or due to the animal's voluntarily action (pre-flight

preparation). This study demonstrates the use of the RNTs for *in vivo* micro-thermography which could potentially acts a powerful tool for investigation of thermogenesis process in small living animals.

Acknowledgements

The author would like to express his deepest gratitude to his supervisor, Asst. Prof. Hirotaka Sato for his dedication, advice, support, and guidance throughout the research.

The author also wishes to honour Prof. Shin'ichi Ishiwata, Prof. Shinji Takeoka, Assoc. Prof. Madoka Suzuki and Dr. Satoshi Arai from Waseda University and Waseda Bioscience Research Institute in Singapore (WABIOS) for their generous support, guidance, and contribution in sharing their ideas and opinions for this project.

Next, the author expresses his appreciation to Mr. Masayuki Tsubaki of WABIOS, Mr. Chew Hock See (CAE Laboratory 2), Ms. Yong Mei Yoke (Materials Laboratory 1), Ms. Koh Joo Luang (Materials Laboratory 2) and Mr. Long Tien Siew (Design Laboratory) of School of MAE, NTU for their support and help during the experiments.

Lastly, the author would like to thank his parents, sibling, relatives, colleagues in WABIOS and Dr. Sato's laboratory and all his friends for their endless support and encouragement throughout this research journey.

Table of Contents

List of Figures

List of Tables

List of Abbreviations and Symbols

Abbreviation	Description
RNT	Ratiometric Nanoparticle Thermosensor
IRT	Infrared Thermography
RIM	Ratiometric Intensity Measurement
UV	Ultraviolet
UV-vis	Ultraviolet-visible
PNIPAM	Poly(N-isopropylacrylamide)
GFP	Green Fluorescence Protein
PS	Polystyrene
PS-MA	Poly(styrene-co-methacrylic acid)
PMMA	Poly(methyl methacrylate)
PMMA-MA	Poly(methyl methacrylate-co-methacrylic acid)
PViCl-PAN	Poly(vinylidenechloride-co-acrylonitrile)
PVA	Polyvinylalcohol
THF	Tetrahydrofuran
EuDT	Eu-tris(dinaphthoylmethane)-bis-trioctylphosphine oxide
$Eu(DBM)_3Phen$	Eu-tris(dibenzoylmethane)-mono(phenanthroline)
EuTTA	Europium thenoyltrifluoroacetonate
$Ir(ppy)_3$	Tris(2-phenylpyridinato-C^2,N) iridium(III)
DLS	Dynamic Light Scattering
NA	Numerical Aperture
DLM	Dorsal Longitudinal Muscle
SD	Standard Deviation
δT	Temperature resolution
ΔT	Temperature shift / change
ΔR	Ratio shift / change
FESEM	Field Emission Scanning Electron Microscope
HAADF-STEM	High-Angle Annular Dark-Field Scanning Transmission Electron Microscopy

List of Publications and Conferences

Original Research Articles:

1. **Ferdinandus**, S. Arai, S. Ishiwata, M. Suzuki, H. Sato "Oral Dosing of Chemical Indicators for *in vivo* Monitoring of Ca^{2+} Dynamics in Insect Muscle", *PLoS ONE* 10.
2. S. Arai*****, **Ferdinandus***, S. Takeoka, S. Ishiwata, H. Sato[#], M. Suzuki[#] "Micro-thermography in millimeter-scale animals by using orally-dosed fluorescent nanoparticle thermosensors", *Analyst* 140: pp.7534-7539.
   *Authors with equal contribution. [#]Corresponding authors.
3. **Ferdinandus***, S. Arai*****, S. Takeoka, S. Ishiwata, M. Suzuki[#], H. Sato[#] "Facilely-fabricated luminescent nanoparticles for microscopic temperature monitoring and mapping in living small animals" *(manuscript in preparation)*.
   *Authors with equal contribution. [#]Corresponding authors.
4. T. Miyagawa, T. Fujie[#], **Ferdinandus**, T. T. Vo Doan, H. Sato[#], S. Takeoka[#] "Stacked Luminescent Ultrathin-sheets Enable High Resolution Ratiometric Temperature Mapping in Living Small Animals" *(manuscript in preparation)*.
   [#]Corresponding authors.

Conference – Poster Presentation:

1. **Ferdinandus**, S. Arai, S. Ishiwata, M. Suzuki, H. Sato (2015) Self-calibrated fluorescent thermometer nanoparticles enable *in vivo* micro thermography in milimeter scale living animals. Solid-State Sensors, Actuators and Microsystems (TRANSDUCERS), 2015 Transducers - 2015 18th International Conference on. pp. 2228-2231. 21-25 June 2015, Anchorage, Alaska, USA.

Chapter 1: Introduction

1.1. Introduction to Ratiometric Nanoparticle Thermosensors (RNT)

Temperature is probably the most important parameter in many industrial fields and scientific studies. It plays a crucial role in governing almost every industrial process. Numerous sensors have been developed in the past decade in order to detect temperature. In the worldwide market, temperature sensors could account to 75-80 % share of the sensor industry.[1] Recent advances in miniaturization of electronic and photonic devices further pushes the needs of precise temperature sensing at the micro- or nanoscale which are typically inaccessible with conventional thermosensors – such as traditional liquid-filled bimetallic thermometers, thermocouples, pyrometers, and thermistors – with fair spatial resolution which are difficult to be scaled down.[2, 3]

In science, particularly for research at the cellular level, temperature provides information about the diverse physiological and chemical activities which occur at different sites in the cell. Several intracellular activities (for instance: cell division, enzymatic reactions, cellular metabolism, and gene expression, etc.) and extracellular stimuli (for example: electrical stimulus, drugs, etc.) may influence the temperature within the cell and cause a deviation from the normal cell temperature.[4] One prominent example is the detection of cancer cells which possess elevated temperature compared to that of normal cells owing to their high metabolism rate.[5-9] Such small scale and brief cellular temperature change requires a high spatial resolution and rapid detection techniques. Therefore, there is

a demand of a sensor system to precisely measure the temperature at the cellular level with the aim to unravel and understand the different physiological and biological activities in cells.

Various high resolution thermometric systems have been developed to address the issue of thermography at the small scale mentioned earlier. These techniques include some advanced optical sensors, such as Infrared thermography (IRT), thermoreflectance, Raman spectroscopy, Scanning thermal microscopy (STM), Transmission electron microscopy (TEM), etc.. Nonetheless, the application of these techniques is limited for *in vivo* application due to their high cost, laborious operation approach, and constrained by the sample characteristics (surface reflectance, emissivity, etc.).[2, 10, 11]

Luminescence sensors have emerged as a potential temperature sensor thanks to their high resolution, rapid response to temperature, as well as high biocompatibility for *in vivo* application. There are different types of approach for luminescence sensors analysis: intensity based analysis,[6, 12-18] lifetime based analysis,[6, 19-22] and anisotropy based analysis.[23-26] Amongst these types of approach, intensity based analysis is superior to the others due to its fast response which is comparable to that of the cellular activities, easy and simple procedure, as well as low cost. However, one should note that intensity based analysis is not spared from the photobleaching, the sample's autofluorescence, the uneven sensor distribution and the intensity change due to Z-axis displacement from the sample.[2, 3, 27]

Ratiometric intensity measurement (RIM) works by using the intensity of another less sensitive luminescence as a reference to that of the temperature sensitive luminescence dye. RIM can aid to cancel out the intensity change due to the inhomogeneous sample distribution and concentration, the surface geometry, and the Z-axis displacement.[12, 15-17, 28] Improvement can also be made by embedding the luminescence sensors into polymeric material in order to increase the photostability of the sensors by blocking contact with oxygen and to prevent cross-sensitivity towards other environmental factors aside from temperature. Moreover, it is possible to embed two dyes into a polymer matrix, allowing RIM analysis, and the size of the particle can be fine-tuned by optimizing the polymer concentration.[3, 6, 29, 30]

The temperature sensitive luminescence sensors are commonly employed for *in vivo* temperature observation at the cellular level.[2, 4, 6, 13, 14, 16, 18, 25, 31-35] Yet, their application into living animals are rare, with the only report covering temperature measurement using Green Fluorescent Proteins (GFP) in *Caenorhabditis elegans*.[24] Still, the application of GFP sensor involves genetic modification in order to load the protein which is constrained by the genetic structure complexity and compatibility of the animal of interest.[36]

This thesis reports the preparation of two ratiometric nanoparticle thermosensors (RNTs) for *in vivo* application, especially in small living animals. The RNTs was generally prepared by the facile nano-precipitation method. The first type of RNT utilized a combination of EuDT as the temperature sensitive dye and $Ir(ppy)_3$ as the less temperature sensitive dye for referencing. Screening was done by utilizing

different types of polymer to find the polymer which form RNT with high stability in the emulsion state and to optimize the size of the RNT. The optimized RNTs were then delivered into *Drosophila melanogaster* (*D. melanogaster*) larvae via oral dosing, which has been proven as an effective way to deliver chemicals into living animals,[37] with an objective to map out the temperature distribution within the larva. The second type of RNT employed EuDT as the temperature sensitive dye, but combined with Rhodamine 800 as the less temperature sensitive dye instead of $Ir(ppy)_3$. This type of RNT was then casted onto *Dicronorrhina derbyana* (*D. derbyana*) beetle flight muscle to monitor the temperature change and distribution during the pre-flight preparation process.

1.2. Objectives

The goal of this project is to develop a high spatial resolution thermosensors for *in vivo* thermography in small living animals. Various types of RNT with different polymers will be prepared using a facile nano-precipitation method to optimize their stability and size. The RNTs will be characterized *in vitro* for their properties and their performance in the *in vivo* application will also be evaluated. Therefore, the objectives of this project are:

- To synthesize and optimize the RNT in terms of their size and stability
- To characterize the RNT for their *in vitro* spectral properties and temperature sensitivity as well as temperature resolution

- To apply the RNT for *in vivo* temperature measurement in small living animals, particularly for *D. melanogaster* larva and *D. derbyana* beetle

1.3. Scope and Limitations

The scope and limitations of this project are:

- The RNTs will be characterized *in vitro* in terms of their fluorescence spectrum intensity for ratiometric analysis
- RNT will be prepared via the facile nano-precipitation method
- The RNTs used for *in vivo* experiments are the ones which display good stability as well as high temperature sensitivity in the *in vitro* analysis
- The subject animals will be:
    - *D. melanogaster* larva owing to the transparent skin which allows luminescence microscopic analysis
    - *D. derbyana* beetle owing to the small body size which reduces object displacement during the muscular activities
- RNT loading will be carried out via oral dosing (for *D. melanogaster* larva experiments) or dropped on top of the muscle of interest, the flight muscle (for *D. derbyana* beetle experiments)

1.4. Significance of the Project

The significances of this project are:

- Temperature measurement in the micro- or nanoscale is commonly performed in the cellular level to observe the activities in cells or organelles within the cell. This project described an attempts to measure temperature in the living organism level which would show unique results as compared to that the cellular level
- The RNTs are able to display a temperature distribution with better spatial resolution within a micro-scale animal, which is impractical by means of conventional IRT and various thermography methods. Therefore, the development of the RNT down to the very small scale will allow a deeper understanding and investigation of thermoregulation and thermogenesis in small living animals

1.5. Organization of Thesis

This thesis consists of 6 chapters. A brief description of each chapter is given below:

Chapter 1 gives the introduction, objectives, scope and limitations, significance of the project as well as the organization of this thesis.

Chapter 2 presents a detailed literature review about this project. A comprehensive overview of various thermography method using infrared thermography and luminescence materials are explained in depth.

Chapter 3 describes the experimental designs and general procedures for RNT preparation, microscopic setup and characterization methods.

Chapter 4 explains about the results and discussions of the *in vitro* characterization of the EuDT–$Ir(ppy)_3$ RNT as well as its *in vivo* application in *D. melanogaster* larvae.

Chapter 5 presents the results and discussions of the *in vitro* characterization of the EuDT–Rhodamine 800 RNT together with its *in vivo* application for temperature monitoring in *D. derbyana* beetle.

Chapter 6 gives the conclusion of the overall results obtained for this project along with the suggestions for future works.

Chapter 2: Literature Review

2.1. Thermoregulation in Insect

Temperature is an important aspect of understanding physiological and behavior of living organisms. In the recent decades, entomologists have been intensely studying how insect behavior and physiological function are affected by temperature. One particular interest is the study of insect thermoregulation or the response of insect body temperature to its environment temperature which depends on the insect's ability to regulate the heat stored within its body. In general, there are two ways in which insect control the thermoregulation: ecothermy (by relying on external source of heat) or endothermy (by generating heat internally through body metabolism).[38]

In most endothermic insects, heat is majorly produced internally at their flight muscles.[38, 39] Interestingly, heat is produced even before flight, during the flight preparation in order to 'warm-up' the muscles via a low-amplitude wing vibration triggered by the simultaneous movement of the antagonist flight muscles.[40-42] During this pre-flight activity, there is no visible movement of the wings, but there are some noticeable changes, such as: an increase in body temperature and oxygen consumption rate.[40, 43-45] Another example of endothermic heat production is the increase of thoracic temperature of a katydid, *Euconocephalus nasutus* due to the contraction of the singing muscles in a similar way as the pre-flight activity described earlier.[46] Thus, it is important to study such a localized heat production, for example at the flight muscles of insects, in order to understand how

thermoregulation is carried out at different local sites in animals which essentially require a temperature sensor with high spatial resolution.

2.2. Infrared Thermography

The pre-flight heat production in insect flight muscles gives an excellent example of localized heat production, down to the microscale. Therefore, it is necessary to have a thermosensor with high spatial resolution and temperature sensitivity to enable observation and investigation at the various local sites. The advances in miniaturization of electronic devices have enable researchers to develop various methods of sensing temperature with high spatial resolution to detect such a local heat production. Asheghi and Yang,[11] and Christofferson[10] have described in detail several high resolution thermal measurement techniques in the micro- to nanometer range, such as: Infrared thermography (IRT), thermal reflectance, Raman scattering, Scanning thermal microscopy (STM), Transmission electron microscopy (TEM), and micro-thermocouple. In this section, IRT will be described in detail as an example for thermography in small animals.

IRT has been commonly employed to map out the temperature distribution in animals for thermographic study.[9, 38, 47-50] IRT has the advantage of non-contact measurement and of large-scale objects observation with a relatively fast process. IRT works by detecting the radiation intensity emitted by the object at a specific wavelength and taking the Planck's black body assumption to determine the absolute temperature.[10, 49, 50] However, IRT comes with some limitations,

such as the low spatial resolution for small objects (high resolution up to the 3-10 µm scale is achievable, but with the help of specially designed lens made of unordinary materials: germanium, sapphire, CaF_2),[28] the incapability to measure temperature of wet samples due to infra-red light absorption by water,[2, 12] and the need to estimate the surface emissivity of the object for temperature calibration.[2, 10] Figure 2-1 below shows that IRT is able to detect the temperature distribution in macro scale objects, such as human hand (a and b), but not in micro scale objects, for example in fruit fly larvae (c and d). Due to these drawbacks of IRT, it is challenging to observe the *in vivo* heat production in small animals. Furthermore, IRT could not be utilized to detect the *in vivo* temperature change in the internal organs of relatively transparent animals, such as fruit fly larvae, as IRT could only detect the surface temperature and unable to penetrate the skin layer of the animal.

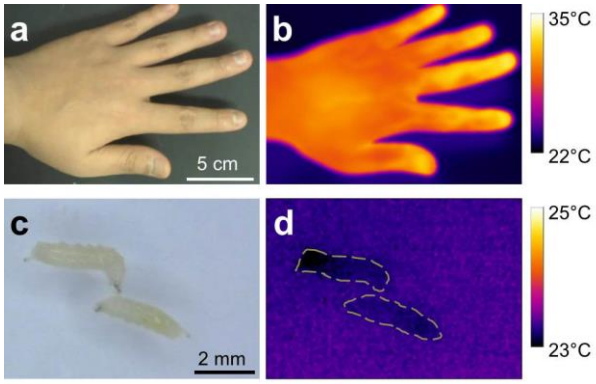

Figure 2-1: Infrared thermography (IRT) images of macro and micro scale objects.[28] Human hand images (a and b) and fruit fly larvae images (c and d) taken by normal camera (a, c) and infrared camera (b, d). The yellow dashed-line (d) indicates the location of the larvae.

To address the shortcomings of IRT, thermal-dependent luminescence materials have been tremendously utilized for *in vivo* temperature sensing up to the nanoscale

level in the past decade owing to their high spatial resolution and detection sensitivity in relatively short time.[2] The next sections will discuss about the details of luminescence sensors for temperature sensing and their applications.

2.3. Luminescence Sensors: Origin of Temperature Dependency

All luminescence molecules (luminophores) theoretically possess temperature dependency owing to the Boltzmann distribution where the temperature dependency of a material is a characteristic of specific electronic band structure within the material itself.[51] Figure 2-2 below depicts the various energy states of electrons for luminescence molecules and the different relaxation pathways of electrons from high energy states to lower energy states. At low temperature, electrons usually sit on their lowest energy state (S_0). Once the material absorbs light energy at a specific wavelength (λ), these electrons are excited to higher energy states (S_1, S_2 or T_1). In order to return to their lowest energy state, the electrons undergo different relaxation pathways, either through radiative transition (emitting energy as light in the form of luminescence, such as fluorescence or phosphorescence), or through non-radiative transition.

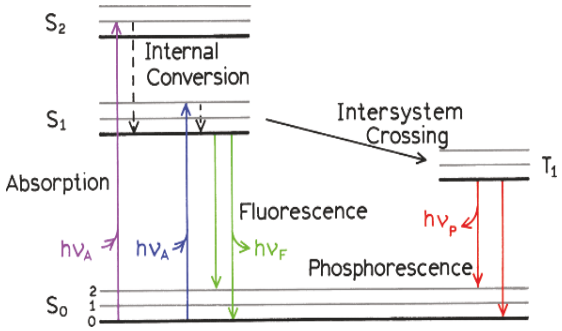

Figure 2-2: Jablonski diagram.[27]

At higher temperature, thermal energy excites electrons at the higher energy states to the electronic states with different vibrational levels, allowing non-radiative relaxation with a rate (k_{nrt}) dependent on temperature following Arrhenius equation as:[3]

$$k_{nrt} \sim e^{\left(-\frac{\Delta E}{k T}\right)} \tag{1}$$

where ΔE is the energy difference between the lowest level of the excited state and the overlap point to a possible non-radiative decay state, and k is the Boltzmann constant. The k_{nrt} rate and the emissive rate (Γ) of a luminescence molecule influence various properties of the luminophore itself, such as: quantum yield (QY), or ratio of the number of photon emitted to the number of excitation photon, lifetime (τ), and intensity (I) following equations 2-4 below as:

$$\mathrm{QY} = \frac{\Gamma}{\Gamma + k_{nrt}} \tag{2}$$

$$\tau = \frac{1}{\Gamma + k_{nrt}} \tag{3}$$

$$I_t = I_0 e^{-\frac{t}{\tau}} \tag{4}$$

where I_t is defined as luminescence intensity at time t and I_0 is the initial intensity.

One should note that in reality, the temperature dependency of a luminophore is more complex than as described above due to its complicated electronic band structure. Temperature also may affect other properties of the luminophore, such as spectral position and shape and polarization. Furthermore, these luminophore properties could also be altered by other environmental factors, aside from temperature, for example: pH,[13, 26, 52, 53] ionic strength,[54] and viscosity.[55,

56] Hence, it is necessary to incorporate the luminophore within an inert material, such as polymer matrixes, to prevent this cross-sensitivity of the luminophore.

2.4. Luminescence Sensors: Measurement Approaches

As described in section 2.3., luminophores generally have several temperature-dependent properties which could serve as indicators for temperature sensing. Some of these temperature-dependent properties of a luminophore are: location of the excitation and emission wavelength,[57] fluorescence lifetime,[22] fluorescence emission intensity,[58] and molecule anisotropy.[59] The most commonly used methods for luminophore temperature sensing are by detecting the change in fluorescence intensity or lifetime.[3] This section aims to give a brief overview of the commonly used methods for temperature sensing using luminophores.

2.4.1. Intensity Based Measurement Approach

The luminescence intensity of a sensor is described by Parker's law as:[27]

$$I = I_0 \Phi k \varepsilon d c \tag{5}$$

where I is the measured luminescence intensity, I_0 is the intensity of the excitation light (laser), Φ is the quantum yield of the luminophore (values from 0 to 1), k is the geometrical factor of the setup used, ε is the molar absorbance of the luminophore, d is the length of penetration, and c is the concentration of the luminophore. From the equation (5) above, the luminescence intensity of a luminophore is ideally only affected by the variation of Φ with temperature. However, in practice, luminescence intensity of a luminophore, particularly for *in vivo* observation, is also affected by

other factors, such as photobleaching, background emission from the sample (autofluorescence), inhomogeneous distribution of the sensor due to surface geometries, and focus drift due to the Z-axis displacement of the sample.[3, 28] Therefore, there is a need of a referenced system in order to negate the change in luminescence intensity of the luminophore.

Ratiometric intensity measurement (RIM) is a commonly used method in intensity based measurement analysis due to the simplicity of the system. RIM analysis has been performed extensively since the first report of intensity ratio analysis for surface temperature measurement performed in 1989.[60] RIM can be used to cancel out the luminescence intensity change due to the uneven sensor distribution, the focus drift from the Z-axis displacement, and the intensity of the light source. However, RIM cannot account for background / autofluorescence correction, light scattering and reflection from the sample.[2, 3, 61, 62] There are two methodologies in RIM depending on the type of sensor used. One method uses the combination of a temperature sensitive dye as an indicator and a less temperature sensitive dye as a reference. Ideally, both dyes should have similar excitation wavelength but display distinct emissions at separate wavelengths. This type of RIM has been popularly utilized, but it suffers from the Förster resonance energy transfer (FRET) and the different photobleaching rate of the two dyes. Thus, careful consideration is needed in choosing the combination of the dyes that will be used for RIM. Another method for RIM uses dual emission wavelength sensors, which are rarely used. The sensor displays temperature dependency in one wavelength and reference signal in the

other, thus making the sensor self-referencing and able to overcome most limitations in RIM.[3]

2.4.2. Lifetime Based Measurement Approach

Aside from the earlier definition described in section 2.3., luminescence lifetime (τ) could also be described as the time for the luminescence intensity of a sensor to drop to the 1/e value of its initial intensity, assuming a single exponential decay.[19] Lifetime based measurement approach offers some advantages over the intensity based measurement approach due to its signal is unaffected with the variation of dye concentrations, sensor size or thickness, sample geometry or surface inhomogeneity, excitation light intensity, as well as photobleaching. Nevertheless, it is difficult to perform lifetime analysis as it need a complicated microscopic setup for signal detection and the sensors need to have a sufficiently long lifetime (μs range) to survive during the observation.[3]

2.4.3. Anisotropy Based Measurement Approach

Luminescence anisotropy is defined by the extent of the polarization of the luminophore emission due to the random Brownian (rotational) motion of the sensor under polarized light. Anisotropy in luminescence sensor arises due to the transition moments for absorption and emission which aligned at specific directions within the luminophore. Under homogeneous solution, luminophores are randomly aligned relative to each other at their ground state. Upon excitation by polarized light source, a fraction of the excited luminophores will have their transition

moments oriented along the vector of the incident polarized light. Figure 2-3 below shows the schematic setup for anisotropy measurement.

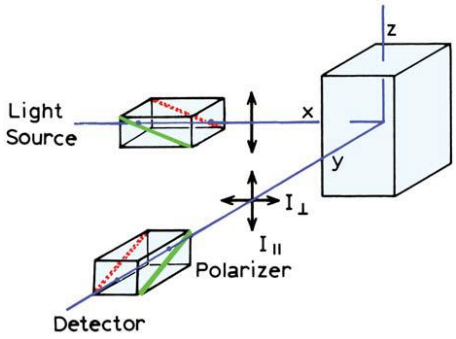

Figure 2-3: Schematic diagram for measurement of fluorescence anisotropies.[27]

Fluorescence anisotropy (*r*) is defined as:[23, 27]

$$r = \frac{I_{\parallel} - I_{\perp}}{I_{\parallel} + 2I_{\perp}} \tag{6}$$

where $I_{\parallel}$ is the emission light intensity when the polarizer is oriented parallel with respect to the excitation light polarizer and $I_{\perp}$ is the emission intensity when the polarizer is arranged perpendicularly. The excited molecules can be depolarized by rotational diffusion of the molecules which can be affected by various factors, one of which is temperature. Upon excitation with polarized light, the emission of the sensor will get lower as the molecules move and rotate at high temperature. Thus, the anisotropy degree (*r*) gets reduced with increasing temperature.[3] [32] This scheme is self-referenced and could give direct absolute temperature read-out. It is also offers some advantages over the intensity based measurement approach as it is independent of sensor concentration, excitation light intensity and does not suffer from photobleaching. However, anisotropy measurement is barely applicable for *in vivo* application in biological samples due to it requires genetic modification to load

into the target samples which is often constrained by the genetic complexity and compatibility of the target sample.[26, 32, 36]

2.5. Types and Applications of Luminescence Sensors for Thermography

Luminescence molecules are the most desirable temperature sensor for *in vivo* application, particularly for cellular imaging, owing to their high spatial resolution and rapid response (comparable to the time scale for various cellular processes). Several desirable properties of a sensor for *in vivo* applications are:[2, 3]

1. High temperature sensitivity: significant signal change with temperature
2. Good photostability to avoid photobleaching and photodecomposition during observation
3. Long wavelength excitation (λ_{ex}) and emission (λ_{em}) in order to avoid phototoxicity of the short UV wavelength or high energy short wavelength visible light as well as to reduce the interference from the autofluorescence of tissues and cells within the similar wavelength range[63-66]
4. High temperature and spatial resolution
5. Display no cross-sensitivity to other parameters aside from temperature, such as: pH, ionic parameters, viscosity of the solution, and interactions with other biomolecules
6. Ratiometric output so as to have the read-out being independent of sensor concentration, uneven sensor distribution, and focus drift due to sample displacement

7. Showing high brightness for detection, and most importantly
8. No toxicity for *in vivo* application

This section will describe some luminescence based sensors for temperature sensing that have been developed in the past decade.

2.5.1. Organic Compounds

Most fluorescence and phosphorescence organic compounds exhibit temperature dependent luminescence, but only some display bright signal with high quantum yield in the solid or fluid phase. In the context of *in vivo* application, it is necessary that the indicators are water soluble, or else they need to be embedded in particles.[31] Some of the most commonly used organic compounds for temperature sensing are shown in Figure 2-4 below.[3]

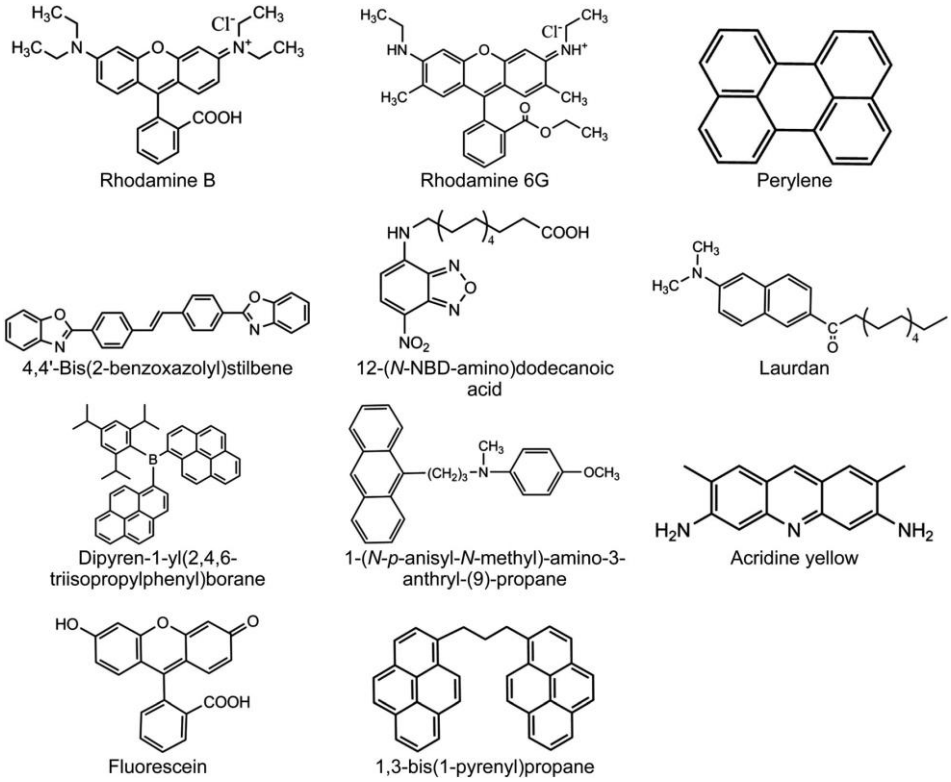

Figure 2-4: Chemical structures of some temperature dependent luminescent organic sensors.[3]

Although some organic molecules displays high temperature sensitivity, their usage suffers from photobleaching and cross-contamination with the surrounding environment which induces the change in intensity due to the other factors aside from temperature.[67, 68] Incorporating these molecules into particles can prevent such drawback, but one must take into account the stability of the polymer-fluorophore to temperature, especially if the sensor is intended to be used at high temperature.[69]

2.5.2. Metal-ligand Compounds

Metal-ligand complexes are other example of the most popularly used sensors for temperature sensing owing to their long lifetime (μs range), excitation in the visible wavelength with adequate brightness and large Stokes shift. However, most of these molecules suffers from oxygen quenching and thus need to be protected by gas impermeable polymers. Some of the reported metal-ligand complexes for temperature sensing are displayed in Figure 2-5 below.[3]

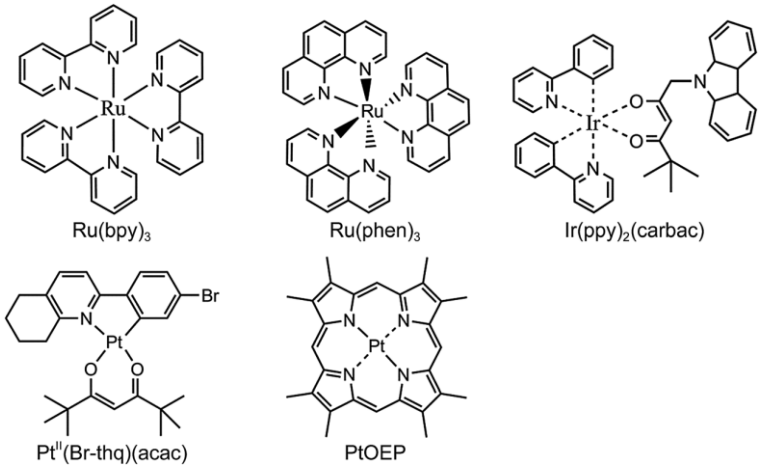

Figure 2-5: Chemical structures of some luminescent metal-ligand temperature sensors.[3]

2.5.3. Lanthanides (Ln^{3+}) Complexes

Some luminescence lanthanide chelate complexes displays sensitivity with temperature, especially the europium(III), Eu^{3+} and terbium(III), Tb^{3+} complexes.[2, 3, 15, 21, 61, 70-72] Single lanthanides (Ln^{3+}) ions without any chelating group absorb light very weakly, which make them unsuitable for temperature sensing. Chelating groups (for example: β-diketonate organic ligands), help to improve absorption via energy transfer from the ligands to the center ion.[20, 70] When chelated, Ln^{3+} complexes could show a long lifetime (several hundred μs up to ms), narrow emission bandwidth, large Stokes shift, with fair brightness. The drawback of these lanthanide complexes is their phototoxicity of excitation in the UV to short wavelength range (350-450 nm). Improvements can be made by increasing the size of the π-electron conjugation system of the chelating groups which can shift the excitation to a longer wavelength. Additionally, these molecules also suffer from photodecomposition under UV irradiation and non-stability in polar solvent (including water). Therefore, they need to be incorporated into polymer matrixes to improve their photostability and stability in polar solvents.[2, 3, 73] Figure 2-6 below shows some lanthanide complexes for temperature sensing.[3]

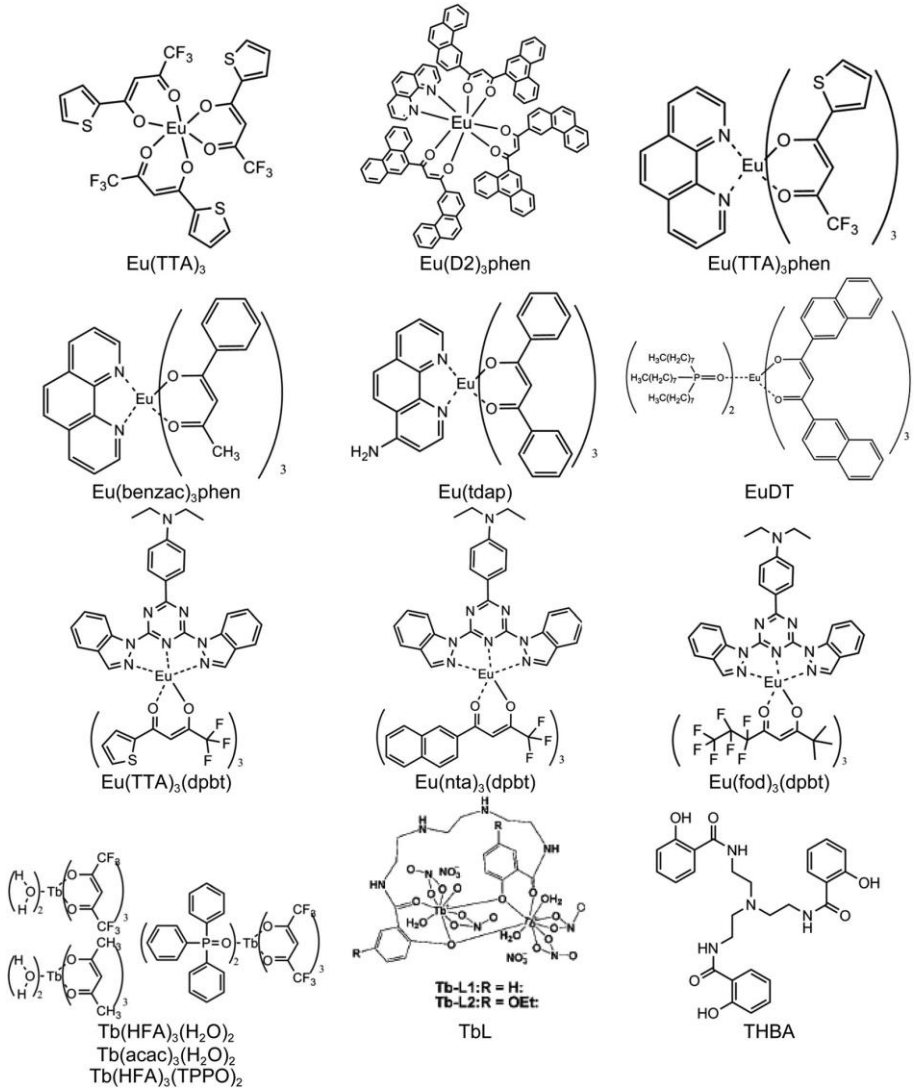

Figure 2-6: Chemical structures of some lanthanide complexes for temperature sensors.[3]

2.5.4. Green Fluorescent Protein (GFP)

Temperature sensitive green fluorescent protein (GFP) is an example of biomolecules for temperature sensing, particularly inside the cells.[24, 25, 32] GFPs work by altering the fluorescence polarization anisotropy of the protein with respect to temperature. This type of sensor shows some benefit for *in vivo* application at the cellular level owing to their biocompatibility, high spatial resolution, fast response, and their capability to target specific organelles in the cell. Nevertheless, little is

known of their application up to the organism level, possibly due to the difficulty in loading GFP into the organism. Up to date, there is only one report of GFP for temperature sensing at the organism level using *C. elegans* as the target animal.[24] Yet, the use of GFP is limited by their loading pathway to the target animal via transgenic operation which is restricted by the genetic complexity of the organism.[36]

2.5.5. Polymeric System

Polymers have been widely used for thermometry, either as active component for sensing temperature, or as passive element to provide physical support and to act as barrier. As active component, polymers–organic dye combination could sense temperature by performing shape transition from the hydrophilic-swollen-globule-state into hydrophobic-collapsed-coil-state in such a way that influence the optical properties of the dye by changing the environment surrounding the dye as illustrated in Figure 2-7.[74] Some examples of such system is Poly(N-isopropylacrylamide) (PNIPAM) and its family under a system defined as nano-gels.[3]

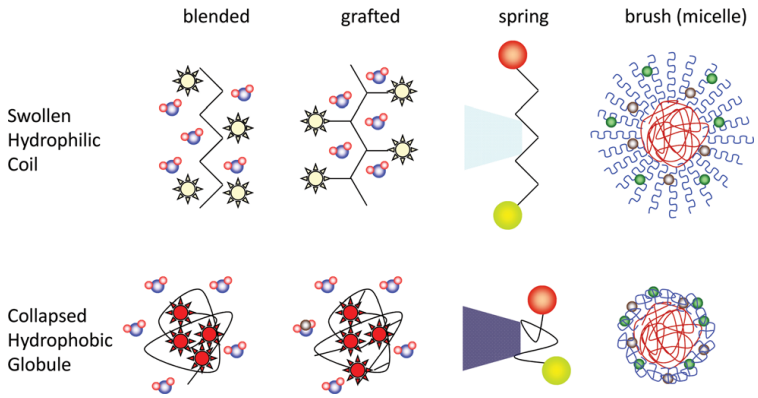

Figure 2-7: Polymer–organic dye thermometer system.[2]

When acting as passive element, polymers are commonly used as supporting media to immobilize and contain temperature sensitive dyes, mainly because they are easy to process and to shape and have good mechanical properties.[75] The polymer is also required to be mechanically and chemically stable with temperature, to securely contain the sensors so that they do not leak out from the polymer matrix, to quickly transfer heat, and not to affect the properties of the sensor.[3] As discussed earlier, many temperature sensitive luminescence dyes are sensitive, not only to temperature, but also to their environment, particularly to oxygen in the air which can quench the luminescence and cause photobleaching, typically in the intensity-based sensors. Therefore, it is essential for the polymers used to contain the dyes to be gas impermeable so as to prevent such cross-sensitivity problem. It is also feasible to incorporate two dyes (temperature sensitive dye and reference dye) into one polymer matrix so that ratiometric system could be achieved. Furthermore, encapsulating the dyes into polymer could also prevent them from interacting with other biomolecules in the cells, which is an advantage for *in vivo* applications.

2.6. Designing the RNT

This section aims to describe the design of the RNTs which were utilized in the projects. In general, intensity based measurement approach coupled with RIM analysis was employed to obtain temperature information. The RIM system with two dyes was utilized as the working principle of our RNT enclosing both a temperature sensitive dye, Eu-tris(dinaphthoylmethane)-bis-trioctylphosphine oxide

(EuDT) and a reference dye. Two reference dyes were employed: tris(2-phenylpyridinato-C^2,N) iridium(III) ($Ir(ppy)_3$) for experiments with *D. melanogaster* larvae and rhodamine 800 for experiments with *D. derbyana* beetle.

The RNTs were prepared via the facile nano-precipitation method in which requires only two different dyes, synthetic polymers as raw materials to comprise the dyes and a hot plate with stirring function. The overall process, including the purification step, could be performed under ambient temperature (maximum 60 °C for this project) and pressure, without the need of complicated experimental setups.[76-78] Furthermore, the whole process could be completed within 2-3 hours which is relatively short compared to other types of thermosensor preparation process.[18, 34, 35]

EuDT was utilized as the temperature sensitive dye in the design of the RNT owing to the superior properties of europium β-diketonate complexes which are commonly utilized as temperature sensing dyes, such as high temperature-dependent emission with a narrow bandwidth, large Stokes' shift and long lifetime (μs range) which is less affected by oxygen.[15, 20, 21, 29, 30, 70, 71] Generally, in most europium chelate complexes, energy from the excitation light will be absorbed by the ligands surrounding the centre Eu^{3+} ion and it will be transferred to the Eu^{3+} ion via the triplet state of the ligand. The metal ion will then emit light as it relaxes back to its lowest energy state. At high temperature, thermal quenching takes place via the non-radiative pathway of relaxation through coupling of the electronic energy level of Eu^{3+} to the environment through molecular vibration. This thermal deactivation process will dominate the relaxation process in the centre Eu^{3+} ion and thus

decreases the overall emission intensity.[70, 79, 80] Earlier reports described the incorporation of Eu-tris(dibenzoylmethane)-mono(phenanthroline) ($Eu(DBM)_3Phen$) and Eu-thenolytrifluoroacetonate (EuTTA) complexes for nanoparticle thermosensors.[14, 16, 17] Nonetheless, the application of these europium complexes for *in vivo* observation was limited by their low photostability and phototoxicity of the UV range excitation. In contrast, EuDT has been reported to be more photostable than EuTTA, have lower phototoxicity with blue light excitation around 400 nm and displays emission at 615 nm. EuDT has a relatively low quantum yield and low stability in the aqueous solution, but these drawbacks are improved by embedding EuDT into a gas impermeable hydrophobic polymer to prevent quenching via photobleaching by oxygen and cross-sensitivity to other environmental factors aside from temperature as described earlier.[3, 15, 29, 70]

As for the first choice of reference dye, a hydrophobic dye $Ir(ppy)_3$ was utilized as a less temperature sensitive dye as it can be excited simultaneously with EuDT (λ_{ex} = 390 nm) but displays distinct emission with λ_{em} peak at 510 nm apart from EuDT. The luminescence intensity of $Ir(ppy)_3$ is less dependent on temperature, thus it can be used as an internal reference coupled with EuDT as the temperature sensitive dye for ratiometric analysis.[81, 82] Both dyes (EuDT and $Ir(ppy)_3$) were embedded into the RNTs prepared using different hydrophobic polymer matrixes to investigate the influence of polymer matrix on RNT size as well as their stability in the emulsion form as shown in Figure 2-8 below. Polyvinylalcohol (PVA, blue shell in Figure 2-8) was added to provide the external hydrophilic layer to further enhance the stability of the RNT in the aqueous solutions.

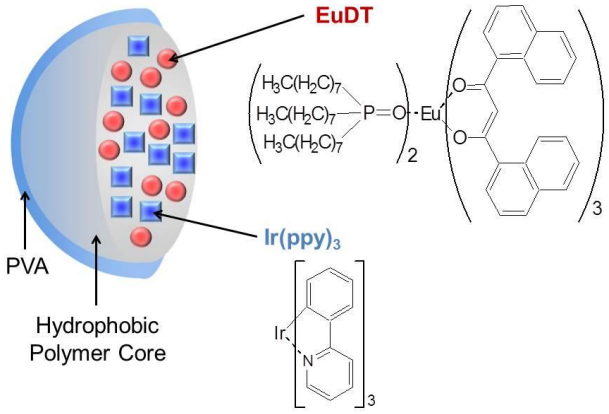

Figure 2-8: Schematic illustration of the RNT structure with EuDT and Ir(ppy)$_3$. The temperature sensitive dye, EuDT (red circles) and the reference dye, Ir(ppy)$_3$ (blue squares) were both embedded in a hydrophobic polymer matrix as the core and further covered with the hydrophobic PVA layer (blue shell) on the outside.

Nonetheless, it was later found that *D. melanogaster* larvae displayed a substantial autofluorescence during microscopic observation under the Ir(ppy)$_3$ channel. Thus, a second option of reference dye, rhodamine 800, was utilized to replace Ir(ppy)$_3$ for preparation of RNT which was to be employed for temperature measurement and monitoring during the pre-flight preparation in *D. derbyana* beetle as described in chapter 5 and illustrated in Figure 2-9 below. Rhodamine 800 is a less temperature sensitive luminescence dye excitable with a low energy long-wavelength visible red light (635 nm) and displays maximum emission (λ_{em} peak) at 710 nm, far from the autofluorescence emission range in the short-wavelength.[83] Therefore, by utilizing a combination of EuDT and rhodamine 800, RIM analysis could be done directly using the measured intensities without the need to subtract the background emission.

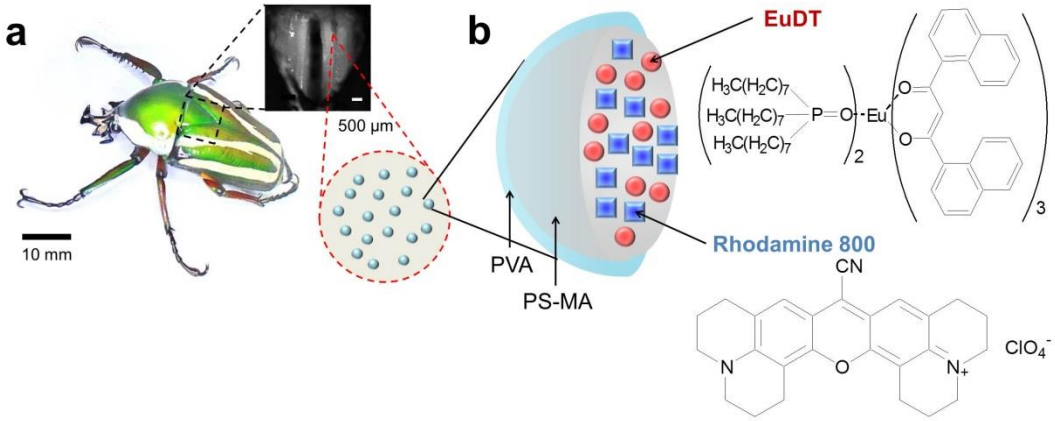

Figure 2-9: Illustration of the RNT loading on *D. derbyana* flight muscle. (a) RNT was loaded into the dorsal longitudinal muscle, a flight muscle (black dashed square, inset) of a *D. derbyana* beetle. (b) Schematic representation of the RNT with the temperature sensitive dye, EuDT (red circles) and the reference dye, rhodamine 800 (blue squares), both embedded in the PS-MA matrix and coated with the hydrophilic layer of PVA (light blue shell).

Chapter 3: Experimental Procedure

3.1. Materials

All chemicals and organic solvents were purchased from Sigma-Aldrich. The different polymers used were: polystyrene (PS) (M_w: 35 000), poly(styrene-*co*-methacrylic acid) (PS-MA) (M_w: 38 000), poly(methyl methacrylate) (PMMA) (M_w: 94 600), poly(methyl methacrylate-*co*-methacrylic acid) (PMMA-MA) (M_w: 34 000), poly(vinylidenechloride-*co*-acrylonitrile) (PViCl-PAN) (M_w: 150 000), and polyvinylalcohol (PVA) (M_w: 13 000-23 000). The reference chemical dyes used were tris(2-phenylpyridinato-C^2,N) iridium(III) ($Ir(ppy)_3$) and rhodamine 800. Whereas the temperature sensitive dye used was Eu-tris(dinaphthoylmethane)-bis-trioctylphosphine oxide (EuDT), synthesized according to earlier report (Shinsei Chemical Company Ltd).[29] Tetrahydrofuran (THF) was used as the organic solvent.

3.2. General RNT Preparation

The RNT was prepared by the nano-precipitation method as described elsewhere.[14, 16] Briefly, the polymer, the temperature sensitive dye (EuDT), and the reference dye ($Ir(ppy)_3$ or rhodamine 800) were dissolved together in THF (1 mL). The mixture was then added quickly into a stirring aqueous PVA solution (20 mg/mL, 8 mL) and left for stirring at 1000 rpm for 1 hour at room temperature. Afterwards, the emulsion was heated to 60 °C for 30-60 mins to completely evaporate the THF solvent. The suspension was then further purified using a

Sephadex PD-10 column (GE Healthcare) under UV light to remove excess dyes and polymers. MilliQ water was used to flush the suspension from the column. Table 3-1 gives the details of the concentration of the polymers and the dyes for EuDT–$Ir(ppy)_3$ RNT. Different polymers were tested to optimize the size of the RNT. Meanwhile for EuDT–Rhodamine 800 RNT preparation, only PS-MA (10 mg/mL) was used with EuDT (1.5 mg/mL) and rhodamine 800 (0.01 mg/mL) as the dyes.

Table 3-1: List of polymers, polymer concentrations, and dyes concentrations for EuDT–$Ir(ppy)_3$ RNT

Polymer	Polymer (mg/mL)	EuDT (mg/mL)	$Ir(ppy)_3$ (mg/mL)
PS	5	1.25	0.15
PMMA	5	1.25	0.15
PS-MA	15	1.5	0.01
PMMA-MA	5	1.25	0.075
PViCl-PAN	15	1.25	0.15

3.3. Size and Characterization of the RNT

The hydrodynamic size of the RNT was measured by a Zetasizer ZSP (Malvern) using dynamic light scattering (DLS) principle. To perform size measurement, 60 µL of the RNT was diluted in MilliQ water to make 1 mL solution.

The luminescence spectrum of the RNT was characterized by a Fluorescence Spectrophotometer (Hitachi F-2700) while monitoring the sample temperature with a thermocouple (TES-1310 type-K, TES Electrical Electronic Corp.). Emission wavelength scan is performed while excitation wavelength is fixed. Sample is prepared by diluting 250 µL of the RNT in MilliQ water to make a 500 µL solution. For EuDT–$Ir(ppy)_3$ RNT, measurement was performed with λ_{ex} at 390 nm as both

dyes can be excited with the same wavelength and emission was recorded from 490 to 650 nm. For EuDT–Rhodamine 800 RNT, measurement of EuDT spectrum was performed with λ_{ex} at 390 nm and emission was recorded from 550 to 650 nm while measurement of rhodamine 800 spectrum was performed with λ_{ex} at 635 nm and emission was recorded from 660 to 750 nm.

The Field Emission Scanning Electron Microscopy (FESEM) was performed by FESEM JOEL 7600F with an acceleration voltage of 5.0 kV and High-Angle Annular Dark-Field Scanning Transmission Electron Microscopy (HAADF-STEM) was performed by FEI Titan 80/300 S/TEM with an accelerating voltage of 200 keV. The Ultraviolet-visible (UV-vis) spectroscopy was performed by Jasco V-670 Spectrophotometer.

3.4. Stereomicroscope Setup

Microscopic imaging was performed by utilizing an Olympus MVX10 Macro Zoom System Microscope coupled with an electron multiplying charged-coupled device (EM-CCD) camera (iXon3 897; Andor Technology) to capture images. A Lumencor Spectra X was used as the light source to illuminate the samples. Two-dimensional images were acquired with an exposure time of 30 msec. Images analysis was performed using ImageJ software (National Institutes of Health).

For EuDT–$Ir(ppy)_3$ RNT observation, an objective lens MVPLAPO 1X with numerical aperture (NA) 0.25 was used for *in vivo* observation of the RNT in larvae while an objective lens MVPLAPO 2XC, NA 0.5 was used for RNT substrate

observation on cover glass slip. An excitation filter FF01-405/10 and a dichroic mirror Di02-R442 were utilized for excitation. A barrier filter FF01-615/24 was used for EuDT channel observation and a barrier filter FF01-520/60 was used for $Ir(ppy)_3$ channel observation. Figure 3-1 below shows the arrangement of the filters as well as the light pathway during the microscopic observation of EuDT–$Ir(ppy)_3$ RNT experiments. The size of the observation field for RNT substrate experiment was 0.84 × 0.84 mm in 512 × 512 pixels, while that for *in vivo* observation of RNT in larvae was 5.22 × 5.22 mm in 512 × 512 pixels. A microwarm plate (Kitazato Science) was utilized to vary the temperature exposed to the object (substrate / larvae). During the stereo microscopic experiment, images were obtained every 2 minutes interval to ensure a stable and uniform temperature of the plate.

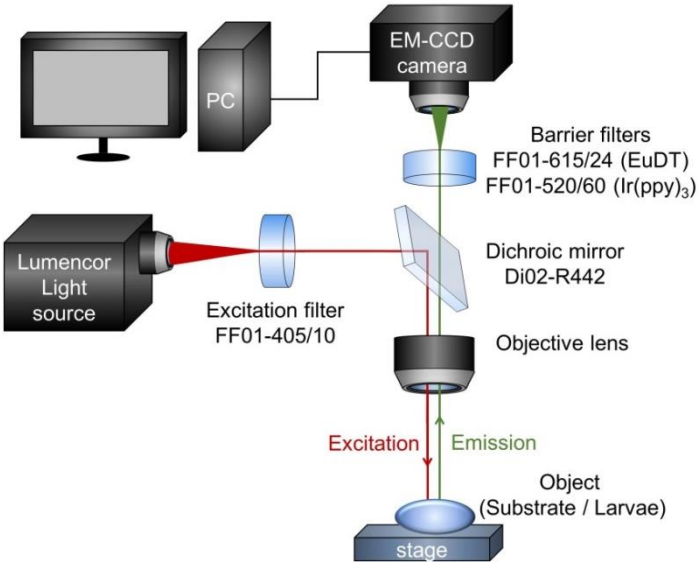

Figure 3-1: Illustration of the stereo microscope setup for EuDT–$Ir(ppy)_3$ RNT observation. One excitation filter was used to excite both EuDT and $Ir(ppy)_3$ whereas two barrier filters were used to selectively collect the emission from the EuDT channel or $Ir(ppy)_3$ channel. The object (particle substrate / larvae) was placed on top of a microwarm plate to subject it to different temperatures.

For EuDT–Rhodamine 800 RNT observation, an objective lens MVPLAPO 1X, NA 0.25 was used for *in vivo* on beetle flight muscle. FF01-405/10 and FF01-640/14 excitation filters were used to excite EuDT and rhodamine 800, respectively. FF01-515/588/700 and FF01-665/150 barrier filters were used to collect the emission from both dyes. A Di01-R405/488/543/635 dichroic mirror was also used to selectively separate the excitation and emission lights. The filters arrangement and the light pathway during the microscopic observation of EuDT–Rhodamine 800 RNT experiments are shown in Figure 3-2 below. The size of the observation field was 3.50 × 3.50 mm in 512 × 512 pixels. Time series images were obtained with a rate of 3 second per frame or 0.33 Hz. Infrared thermography (IRT) measurement was done by using a Fluke Ti400 infrared camera with an observation field size of 320 × 240 pixels and a frame rate of 9 Hz. External heating of flight muscle for *in vivo* calibration of the RNT on the muscle was carried out using a diode-pumped solid-state 980 nm CW laser connected with a flexible optical fibre to a collimating lens (5 mm ⌀ spot size) (Viasho).

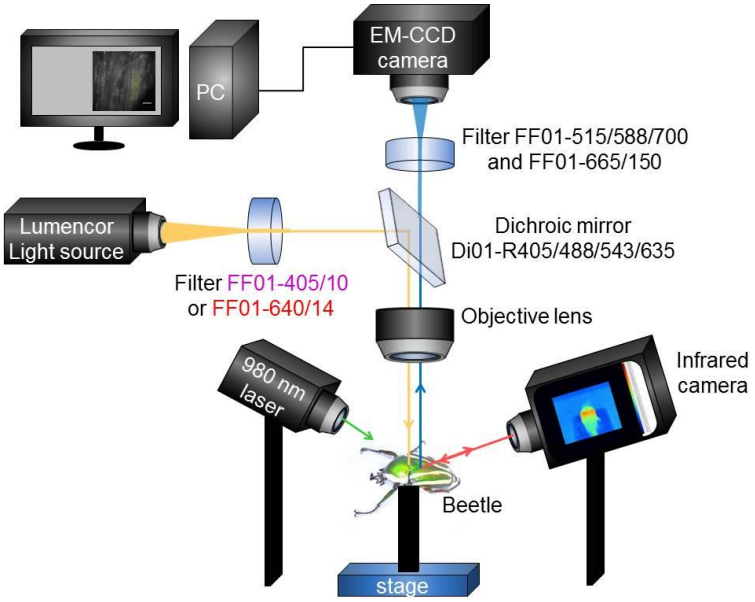

Figure 3-2: Illustration of stereo microscope, laser, and infrared camera setups for EuDT–Rhodamine 800 RNT observation. The excitation filter in purple font was used to excite EuDT whereas the excitation filter in red font was used to excite rhodamine 800. The beetle was tethered on top of a stick which was fixed to a metallic stage. The flight muscle was exposed and observed under stereo microscope. External heating was induced by using a 980 nm laser. The temperature of the muscle was monitored by an infrared camera.

3.5. Study Animals

Laboratory wild-type *Drosophila melanogaster* Canton Special (CS) strain larvae were selected for *in vivo* oral dosing experiment. The larvae were fed with a mixture of fly food (Nutri-Fly BF, 20 ml), replaced with new food weekly. The average size of *D. melanogaster* larva is 5-7 mm. The larvae were left to grow and evolved within in a closed tube covered with cotton cap to prevent the fly to escape.

Dicronorrhina derbyana (Coleoptera: Scarabaeidae) were used as the insect model for temperature monitoring during the pre-flight preparation. The size and weight of one *D. derbyana* beetle are approximately 40 mm and 3 g, respectively. The beetles

were kept in separate plastic terrariums (20 cm × 15 cm × 15 cm) with tissue paper as the base and were fed with a cup of sugar jelly (Lai Bao Food Co., Ltd) weekly. The temperature and relative humidity in the terrariums were maintained at 23 °C and 50 %, respectively.[84] After any experiments, the tested beetles were returned back to the terrarium, cared and fed under the same conditions as before the experiments until they ended their lives. The use of beetles is permitted by the Agri-Food & Veterinary Authority of Singapore (AVA, HS code: 01069000, Product code: ALV002). Invertebrates including insects are exempt from the ethics for animal experimentation according to National Advisory Committee for Laboratory Animal Research (NACLAR) Guidelines.

3.6. *In vivo* Experiments of EuDT–Ir(ppy)$_3$ RNT with *D. melanogaster* Larva

Prior to the *in vivo* observation, some *D. melanogaster* larvae were kept and dosed in separate tubes containing a mixture of 50 μL of the RNT and 50 μL of the fly food for 2 days. After dosing, the larvae were washed with insect medium (Grace's Insect Medium, unsupplemented, Thermo Fisher, 50 μL) in order to remove the RNT attached on the larvae's skin. The larvae were then placed on top of a glass cover slip and anaesthetized using cotton balls dipped in chloroform. The glass cover slip was then set on top of a microwarm plate to alter the surrounding temperature of the larvae as shown in Figure 3-1. During the stereo microscopic experiment, images were obtained every 2 minutes interval to ensure a stable and uniform temperature of the plate.

3.7. *In vivo* Experiments of EuDT–Rhodamine 800 RNT with *D. derbyana* Beetle

The *in vivo* experiments using *D. derbyana* beetle were conducted by tethering the beetle on the top of a stick which was fixed to a metallic base as shown in Figure 3-2. The front and mid legs of the beetle were dissected, leaving the two hind legs with the tarsus removed in order to minimize the beetle's movement during microscopic observation. The cuticles above the beetle's dorsal longitudinal muscle (DLM) were removed to expose the muscle (black dashed square in Figure 2-9a). A buffer solution containing the RNTs was then cast to cover the whole exposed area of the muscle.

In vivo calibration of the RNT on the muscle was carried out by heating up the muscle using a 980 nm laser (Figure 3-2). Water molecules in the muscle absorbs the light at 980 nm, and consequently, the muscle was externally heated up by the laser.[85] The temperature of the muscle was raised in a step-wise manner by increasing the laser power with 2 minutes waiting interval between different laser powers, while a homogeneous temperature over the muscle was ensured by IRT. Microscopic images of the muscle were acquired after the 2 minutes waiting interval. The muscle was then allowed to cool down naturally while the laser power was reduced in a similar step-wise manner every 2 minutes interval.

To trigger the pre-flight preparation of the beetle, a mechanical stimulus was applied, i.e., gently pinching one of the hind legs with a pair of tweezers. The flight

muscles were then activated to warm up as the beetle's response to the stimulus applied. The beetle was then left to naturally cool down to room temperature.

Chapter 4: Results and Discussions of EuDT–$Ir(ppy)_3$ RNT

4.1. RNT Preparation with Different Polymers and Particle Size

Different polymer matrixes (Table 3-1), such as PS, PMMA, PS-MA, PMMA-MA, and PViCl-PAN were used to prepare RNT containing EuDT and $Ir(ppy)_3$. Screening was done to investigate the influence of different polymer matrixes on the RNT size as well as their stability in the emulsion form. Figure 4-1 below show the chemical structures of the various polymers utilized.

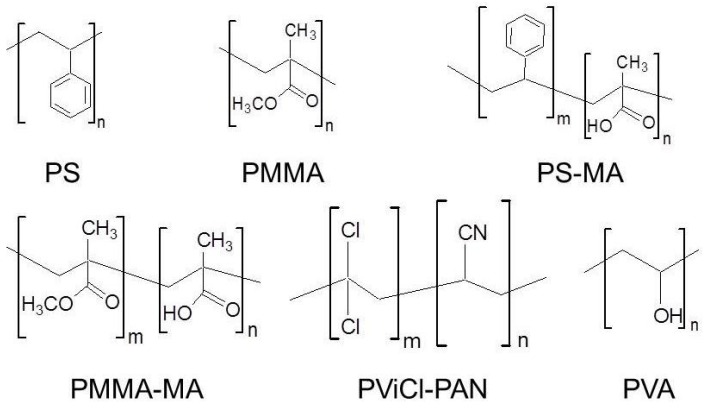

Figure 4-1: Chemical structures of the polymers used for RNT formation.

Among these polymers, the PS and PMMA polymers could not form RNT as precipitation occurs during the particle formation process, but the other polymers successfully formed stable suspension of RNT. This could be associated to the lack of carboxylic group in PS and PMMA which leads to a poor solubility of the emulsion in aqueous PVA solution. On the other hand, the carboxylic group in PS-MA and PMMA-MA as well as the nitrile group of PViCl-PAN oriented towards the surrounding water molecules while PVA, as a charge-free polymer, provide a hydrophilic outer layer of the nanoparticle which enhance the formation of a stable suspension.

The hydrodynamic diameter of the prepared PS-MA, PMMA-MA and PViCl-PAN RNT were determined by using Zetasizer. Figure 4-2 below shows the size distribution of the RNT while the measured size from the number population is given in Table 4-1.

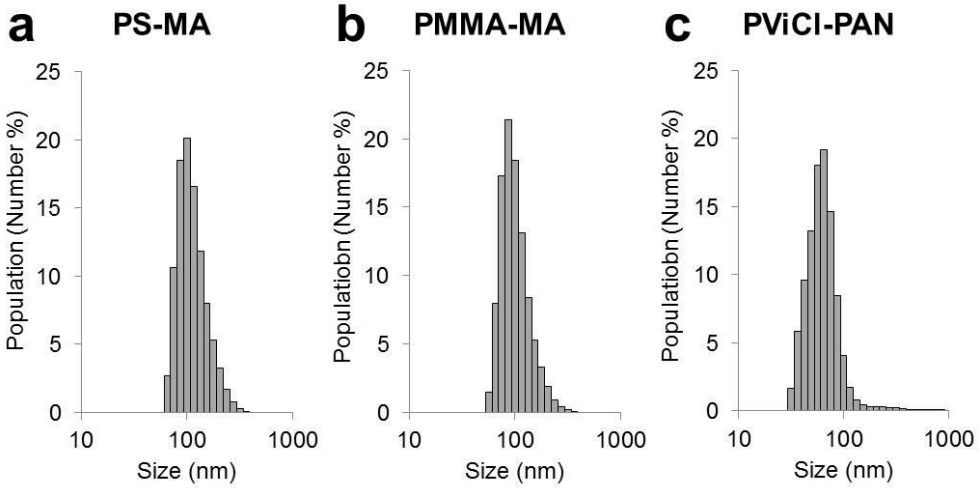

Figure 4-2: Size distribution of the RNTs prepared with different polymers. (a) PS-MA, (b) PMMA-MA, and (c) PViCl-PAN.

Table 4-1: Hydrodynamic diameter of the RNTs prepared with different polymers. NF means no particle is formed.

Polymer	Hydrodynamic diameter (nm)
PS	NF
PMMA	NF
PS-MA	124 ± 45
PMMA-MA	110 ± 40
PViCl-PAN	69 ± 39

4.2. *In vitro* Temperature Sensitivity

For screening purpose, the *in vitro* temperature sensitivity was measured by recording the spectrum of the RNT at different temperatures. It was observed that the luminescence intensity of EuDT (λ_{em} peak at 615 nm) as the temperature sensitive dye decreases with increasing temperature, while that of the reference dye,

$Ir(ppy)_3$ (λ_{em} peak at 506 nm), was less influenced by temperature change (Figure 4-3 a,c,e). This finding follows the phenomenon of thermal quenching in europium β-diketonate complexes, particularly in EuTTA as reported earlier.[20, 70, 79, 80]

For ratiometric analysis, the ratio of luminescence intensity of EuDT (I_{615}) to that of $Ir(ppy)_3$ (I_{506}) was calculated. The ratio (I_{615}/I_{506}) at each temperature was then normalized to the ratio at 37 °C and plotted against temperature (Figure 4-3 b,d,f). The temperature sensitivity of the RNT was defined as the gradient of the (I_{615}/I_{506}) versus temperature plot. Table 4-2 summarizes the temperature sensitivity of the different RNTs prepared. It was observed that the RNTs' sensitivity differs with different polymer matrixes with PS-MA RNT showing the highest sensitivity of 0.039 /°C. This result infers that different polymer matrixes might influence the rate of energy transfer from the dinaphthoylmethane (β-diketonate) ligand to the centre Eu^{3+} ion of EuDT and thus altering the temperature sensitivity, although the mechanism is still unknown. Furthermore, the PViCl-PAN RNT was found not stable under long term (>1 week) storage as the particles sunk to the bottom of the solution in a glass bottle. Thus, for further experiments and analysis, only PS-MA and PMMA-MA RNTs were utilized.

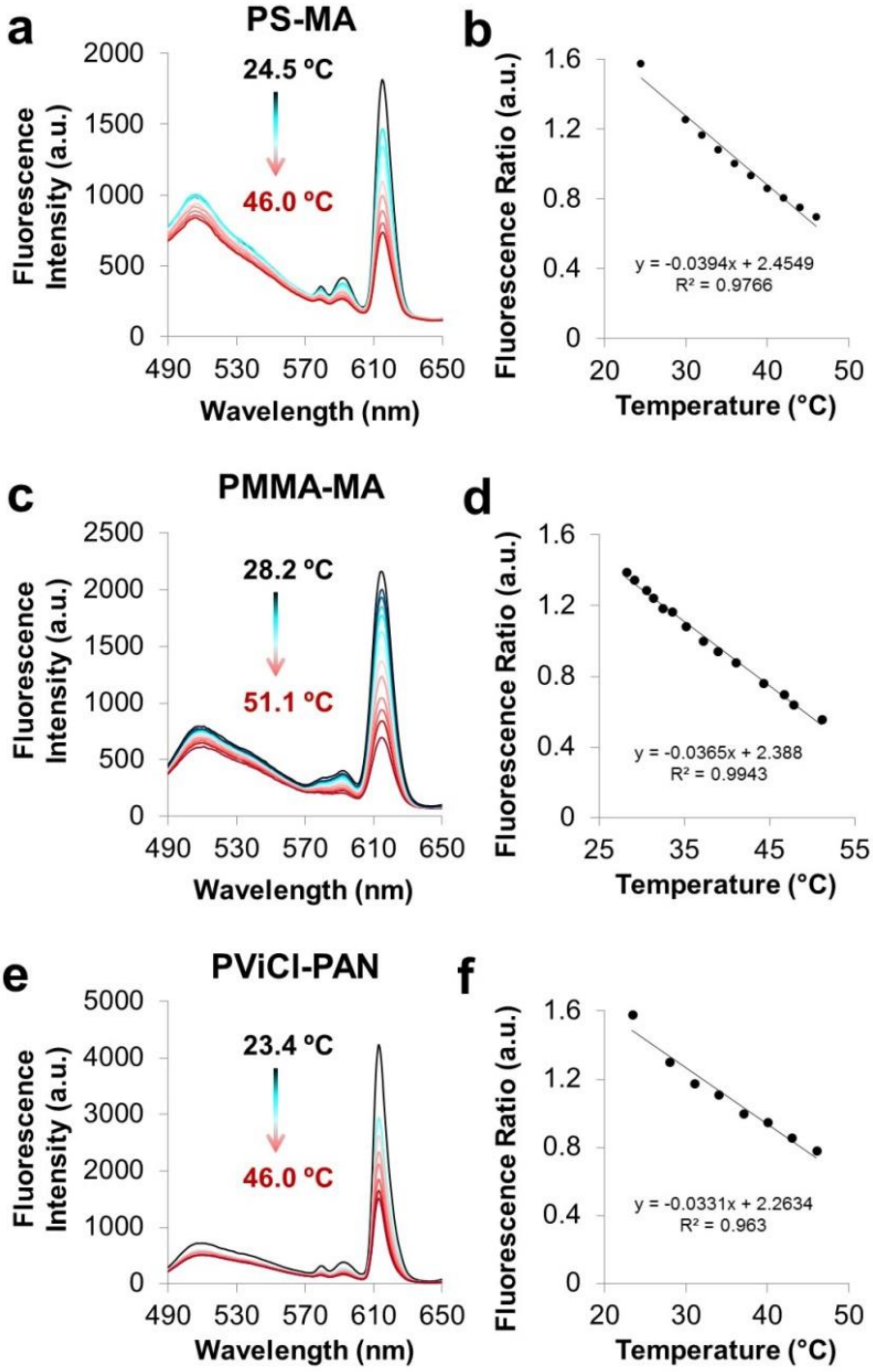

Figure 4-3: *in vitro* temperature sensitivity measurement. (left) Luminescence spectrum of the RNTs measured at various temperature and (right) luminescence intensity ratio (I_{615}/I_{506}) plot versus temperature for various polymers: (a, b) PS-MA, (c, d) PMMA-MA, and (e, f) PViCl-PAN. The excitation wavelength was set at 390 nm and the emission was recorded from 490 to 650 nm. The intensity ratio (I_{615}/I_{506}) is normalised to the ratio value at 37°C.

Table 4-2: Sensitivity of RNTs prepared from various polymers

Polymer	Temperature Sensitivity (/°C)
PS-MA	0.039
PMMA-MA	0.036
PViCl-PAN	0.033

The PS-MA RNT as the RNT showing the highest temperature sensitivity was further verified under stereo-microscope. Sample was prepared by casting a buffer solution containing the RNT on a glass cover slip and drying overnight. Single dots of the RNT particle was observed under the EuDT and $Ir(ppy)_3$ channels (Figure 4-4a). The dried sample was then heated from 26 to 44 °C and the variation in luminescence intensity of the RNT was recorded. The luminescence intensity was analyzed from the region of interest (ROI) enclosing a single dot (Figure 4-4a) and the ratio intensity (EuDT/ $Ir(ppy)_3$) was plotted at each temperature as shown in Figure 4-4b. To calculate the sensitivity of the RNT, the mean ratio intensity measured from different ROIs (n = 12 ROIs) with SD was plotted against temperature (Figure 4-4c). The sensitivity, taken from the gradient of the plot, was calculated as –0.021 /°C, less than that measured during the cuvette experiment discussed earlier in section 4.1 (–0.039 /°C). The lower sensitivity observed for the substrate observation could be attributed to the variation in fluminescence intensity of the RNT measured by different setups as affected by numerous factors, such as: excitation light intensity, sensor sensitivity or gain, and emission bandwidth. This result infers that it is necessary to calibrate the RNT with different setups. It was also observed that the RNT response to the varying temperatures during the re-cooling process (from 44 to 26 °C, blue dots in Figure 4-4c) was similar to that

during the heating process (from 26 to 44 °C, red dots in Figure 4-4c). This shows that the RNT could response reversibly with temperature and photobleaching is insignificant.

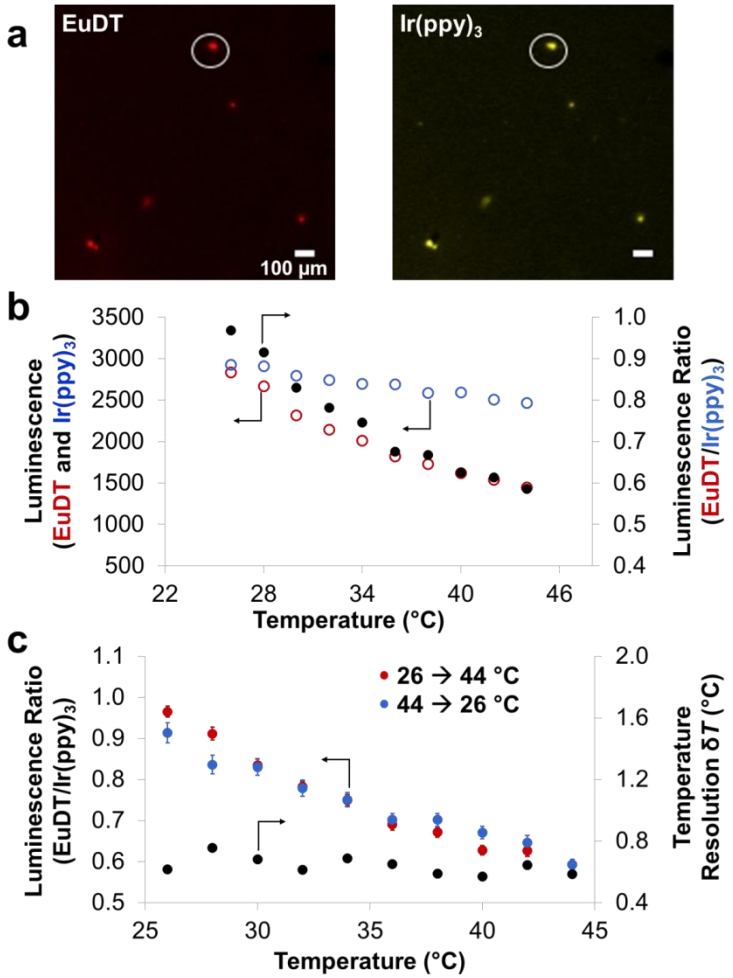

Figure 4-4: Stereo microscopic observation of the PS-MA RNT on glass cover slip. (a) False-colour luminescence images of the RNTs under EuDT channel (left) and $Ir(ppy)_3$ channel (right). Scale bars: 100 µm. (b) Luminescence intensity of a single RNT dot measured from the region of interest (ROI) depicted in (a) under EuDT (red open circle) and $Ir(ppy)_3$ (blue open circle) channels was plotted at different temperatures. The luminescence ratio (EuDT/ $Ir(ppy)_3$) was plotted as black dots. (c) The average of the ratio of different ROIs (n = 12 ROIs) was plotted against temperature, during heating process (from 26 to 44 °C, red dots) and cooling process (from 44 to 26 °C, blue dots). The temperature sensitivity, or the gradient of the slope obtained from the heating process is –0.021 /°C ($y = -0.021x + 1.5$, $R^2 = 0.96$). The temperature resolution or δT, defined as the SD divided by the temperature sensitivity (–0.021/°C), was plotted as black dots.

One important feature of the RNT is its temperature resolution (δT) which tells the accuracy of the measurement. Temperature resolution at each temperature [δT(T)] is calculated from the standard deviation (SD) of the ratio intensity divided by the sensitivity of the RNT (–0.021 /°C).[5, 6] The PS-MA RNT shows a temperature resolution of 0.5 to 0.8 °C (black plots in Figure 4-4c) within the examined temperature range (26 to 44°C) which is comparable to the other previously reported luminescence sensor for thermometry.[5, 16]

4.3. *In vivo* Temperature Measurement in *D. melanogaster* Larva

The prepared RNTs were examined further for temperature mapping *in vivo* by orally dosing *D. melanogaster* (fruit fly) larvae with the RNTs. Fruit flies at their different stages of life (larvae, pupae, or adult fly) have been extensively used as a typical animal for physiological and biological studies. Fruit fly larvae were chosen as the subject animal for our micro-thermography due to their relatively transparent body which enables a facile *in vivo* study. Loading of the RNTs were tested via oral dosing of PS-MA RNT and PMMA-MA RNT as the two RNTs which show good stability in the emulsion state and high temperature sensitivity during screening at the *in vitro* cuvette experiments. Oral dosing have been demonstrated as a facile pathway to load and deliver chemicals into insects without the need for surgical operation or injection of the chemicals.[37] The larvae were dosed with a mixture of fruit fly food solution and the RNT solution for 2 days prior to observation. The larvae were then exposed to varying external temperature by placing the larvae on

top of a glass coverslip over a microwarm plate. Figure 4-5 shows the microscopic images of the dosed larvae as well as the control (non-dosed) larvae taken at different temperatures.

The RNTs were observed mainly localized at the gut of the larvae as the main pathway for absorption and digestion of food in insects.[86] It was noted that there was a considerable amount of background signal due to the autofluorescence of the tissue observed particularly in the $Ir(ppy)_3$ channel, while such background signal was significantly low in the EuDT channel (Figure 4-5). Similar to the *in vitro* substrate experiment, the RNT dosed larvae showed a decrease of luminescence intensity in the EuDT channel while that of the $Ir(ppy)_3$ channel was constant. The averages of the ratio intensity measured from various ROIs in different RNTs dosed larvae and the control larvae were plotted against the external temperature in Figure 4-6. Similar trend of the curve slope was also observed during the heating process (from 26 to 44 °C, red dots in Figure 4-6) as compared to that of the PS-MA substrate case. The RNTs reversibility was also observed as the mean ratio increased with decreasing temperature (from 44 to 26 °C, blue dots in Figure 4-6). The signal of autofluorescence in both the EuDT and the $Ir(ppy)_3$ channels were non-dependent on temperature as the ratio intensity measured from the control larvae was rather flat as shown in Figure 4-6c. The δT was also defined for the larvae dosed with PS-MA RNT and PMMA-MA RNT. Table 4-3 summarizes the temperature sensitivity of the RNT (taken from the curve slope during the heating process) for the RNT-dosed larvae and the control larvae as well as their respective δT.

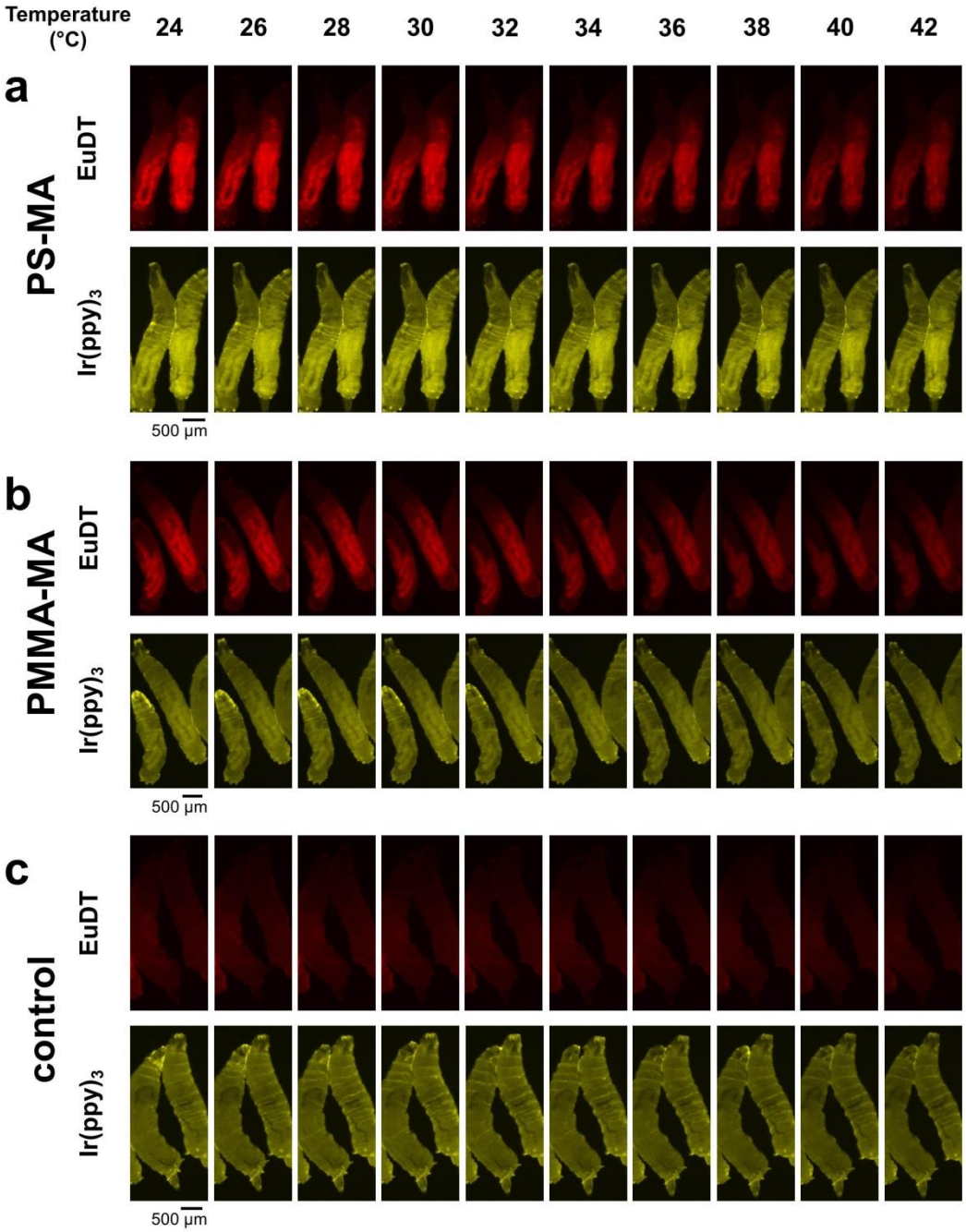

Figure 4-5: Luminescence stereo microscopic observation of the fruit fly larvae orally dosed with the RNTs at varied temperatures. (a) PS-MA (b) PMMA-MA and (c) control (non-dosed) larvae, all observed in the EuDT channel (upper panels) and the $Ir(ppy)_3$ channel (lower panels) shown in false colours.

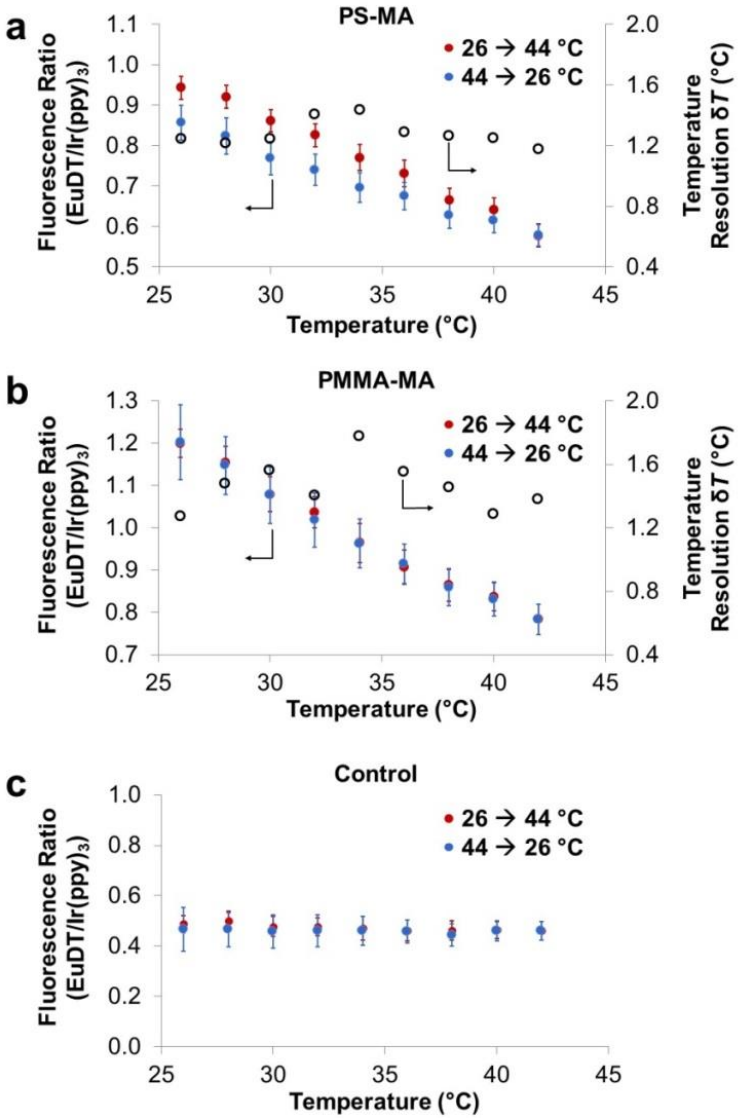

Figure 4-6: The averaged luminescence ratio plot at each temperature for RNTs orally dosed fruit fly larvae. The average of the ratio of different ROIs: (a) PS-MA (n = 12 ROIs), (b) PMMA-MA (n = 10 ROIs), and (c) control (non-dosed) larvae (n = 12 ROIs) was plotted against temperature, during heating process (from 26 to 44 °C, red dots) and cooling process (from 44 to 26 °C, blue dots). The calibration slopes during the heating process for the different RNTs are: (a) PS-MA: –0.023 /°C (y = –0.023x + 1.5, R^2 = 0.99), (b) PMMA-MA: –0.026 /°C (y = –0.026x + 1.9, R^2 = 0.99) and (c) control: –0.0022 /°C (y = –0.0022x + 0.55, R^2 = 0.77). The temperature resolution or δT, defined as the SD divided by the temperature sensitivity, was plotted as black dots.

Table 4-3: Slope of the heating curve of control larvae and larvae dosed with RNTs and their respective δ*T*. N.A. means data is not available.

Larvae Dosed	Slope of the Heating Curve (/°C)	δ*T* (°C)
PS-MA	–0.023	1.2 to 1.4
PMMA-MA	–0.026	1.2 to 1.8
Control	–0.0022	N.A.

The slight difference in the slope of the heating curve for the larvae dosed with the two RNTs as compared to the PS-MA substrate sensitivity on a glass cover slip could be associated to the environmental difference between the substrate and the RNTs in the gut of the larvae. Both results of the *in vitro* substrate experiment and the *in vivo* experiment in fruit fly larvae give similar temperature senstivity results which support the idea of temperature specific dye-embedded polymeric nanoparticles could operate in different extreme environments. This *in vivo* observation of the RNT in larvae could work as an example of dye-embedded polymeric nanoparticle as temperature sensor for *in vivo* application.

It should be noted that there is a larger value of δ*T* for the RNTs dosed larvae as compared to the PS-MA RNT substrate (section 4.2) even though same microscopy setup was utilized in both case. The larger δ*T* value in the larvae experiment suggests that temperature might be distributed heterogeneously within the larvae body. Therefore, the RNT system could works as a thermosensor for micro thermography to indicate such millimeter scale temperature distribution in small animals which is undetectable by commercially available IRT.[28] Nonetheless, the large δ*T* in the *in vivo* application of the EuDT–$Ir(ppy)_3$ RNTs could not be assigned to the internal temperature distribution alone. Autofluorescence interference in the $Ir(ppy)_3$ channel may cause an under- or overestimation of the

intensity ratio value resulting in a large SD and δT. Therefore, there is a need of a RNT system which shows emission away from the autofluorescence range of tissue in the short blue to green wavelength, for example in the far long infrared wavelength.[7, 64, 65] One such dye is rhodamine 800 which will be described in details in the next chapter.

Chapter 5: Results and Discussions of EuDT–Rhodamine 800 RNT

5.1. RNT Size and *in vitro* Temperature Sensitivity

The EuDT–Rhodamine 800 RNT was prepared only using the PS-MA as the polymer which produced the EuDT–$Ir(ppy)_3$ RNT with the highest temperature sensitivity during the *in vitro* screening with different polymers as described earlier in section 4.2.. The hydrodynamic diameter of the RNT was measured as 70 ± 23 nm by Zetasizer (Figure 5-1a). The measured RNT diameter also agrees with the particle size as observed under Field Emission Scanning Electron Microscope (FESEM) and High-Angle Annular Dark-Field Scanning Transmission Electron Microscopy (HAADF-STEM) (Figure 5-2). We could also note that EuDT was embedded in the PS-MA matrix from the HAADF-STEM image (Figure 5-2b) as displayed as bright dots which corresponds to the atoms with high Z-value.[87, 88] Additionally, UV-vis absorption spectrum of the RNT-embedded dyes and PS-MA only particle were recorded to determine the loading of the dyes in the RNT as shown in Figure 5-3. From the UV-vis absorption spectrum, it could be confirmed that the dyes were embedded in the polymer owing to the absorption peaks of both EuDT and rhodamine 800 at 370 nm and 700 nm, respectively, recorded from the RNT-embedded dyes spectrum (red lines in Figure 5-3).

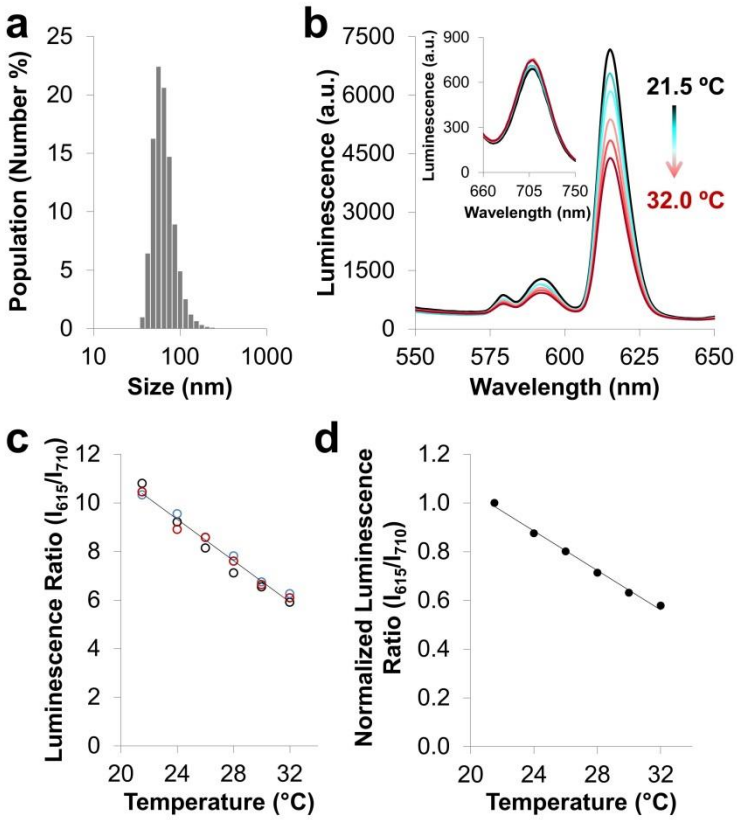

Figure 5-1: RNT size and temperature sensitivity. (a) Size distribution of the RNT, average size = 70 ± 23 nm (DLS measurement). (b) EuDT emission spectra (λ_{ex} = 400 nm) of the RNT at varied temperatures (from 21.5 °C to 32.0 °C). Inset: Rhodamine 800 emission spectra (λ_{ex} = 635 nm) of the RNT. (c) The ratio of luminescence intensity of EuDT to that of rhodamine 800 (I_{615}/I_{710}) was plotted (n = 3 trials, different colours represent independent trials) against the temperature. The temperature sensitivity or the gradient of the averaged data (black line) is –0.43 /°C ($y = –0.43x + 19.56$, $R^2 = 0.99$). (d) The normalized luminescence ratio (I_{615}/I_{710}) plotted against the varying temperature. The ratio at each temperature was normalized by the ratio at 21.5 °C. The normalized temperature sensitivity is –4.0 %/°C relative to 21.5 °C ($y = –0.040x + 1.86$, $R^2 = 0.99$).

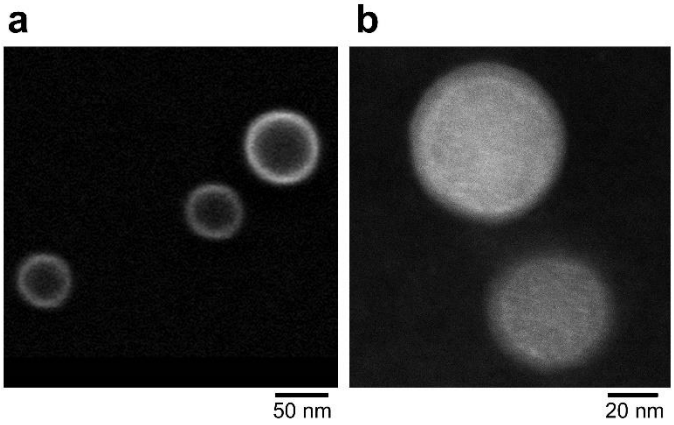

Figure 5-2: Electron Microscopy Images of the prepared RNT. (a) Field Emission Scanning Electron Microscopy (FESEM) image. (b) High-Angle Annular Dark-Field Scanning Transmission Electron Microscopy (HAADF-STEM) image.

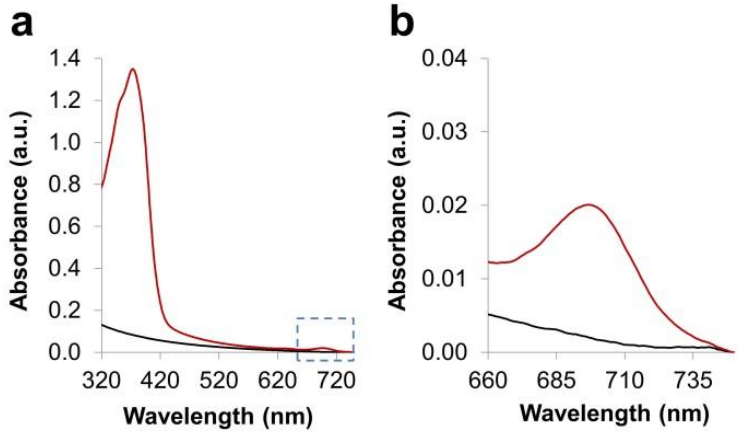

Figure 5-3: UV-vis absorption spectra of the RNT. The average (n = 5 measurements) absorption spectra of EuDT and rhodamine 800 embedded PS-MA particles (red lines) and PS-MA particles without dyes (black lines). (a) The peak at 370 nm corresponds to the EuDT absorption. The blue rectangular indicates the rhodamine 800 absorption as displayed in the magnified image in (b). (b) The peak at 700 nm corresponds to the absorption of rhodamine 800.

For the *in vitro* temperature sensitivity analysis, the maximum emission intensity was obtained for both EuDT at 615 nm (I_{615}) and rhodamine 800 at 710 nm (I_{710}) at varied temperatures (from 21.5 °C to 32.0 °C) as shown in Figure 5-1b. The ratio of intensity of EuDT to that of rhodamine 800 (I_{615}/I_{710}) was then plotted against the varied temperatures (Figure 5-1c) and the temperature sensitivity, defined as the gradient of the I_{615}/I_{710} plot, was –0.43 /°C. Such temperature sensitivity was

measured as –4.0 %/°C relative to 21.5 °C (Figure 5-1d) in the tested temperature range from 21.5 °C to 32.0 °C which is comparable to or higher than that of earlier reported RNTs.[12, 14, 16, 17, 28, 71] Note that the small tested temperature range (21.5 °C to 32.0 °C) was examined owing to the temperature range in which the pre-flight preparation in *D. derbyana* beetle occurs. For other applications, the emission spectrum and temperature sensitivity of the RNT in a wider temperature range (21.5 °C to 44.0 °C) was also checked (Figure 5-4).

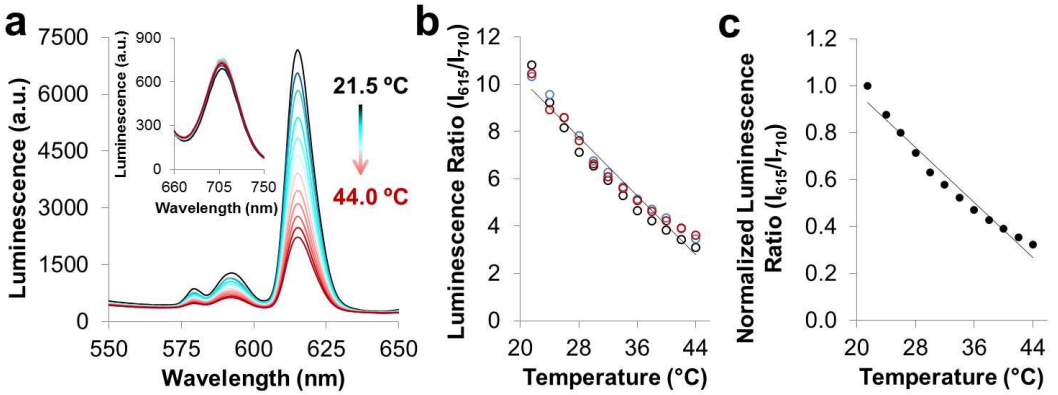

Figure 5-4: The *in vitro* normalized luminescence ratio (I_{615}/I_{710}) measured between 21.5 °C to 44.0 °C. (a) EuDT emission spectra (λ_{ex} = 400 nm) of the RNT at the varied temperatures. Inset: Rhodamine 800 emission spectra (λ_{ex} = 635 nm) of the RNT. (b) The ratio of luminescence intensity of EuDT to that of rhodamine 800 (I_{615}/I_{710}) was plotted (n = 3 trials, different colours represent independent trials) against the varied temperatures. The temperature sensitivity or the gradient of the averaged data (black line) is –0.31 /°C (y = –0.31x + 16.45, R^2 = 0.97). (c) The ratio at every temperature was normalized by the ratio at 21.5 °C. The temperature sensitivity of the normalized ratio is –3.0 %/°C relative to 21.5 °C (y = –0.030x + 1.56, R^2 = 0.97).

The RNT displayed reversible luminescence intensity ratio at the varied high and low temperatures (Figure 5-5) and also observed in N_2 saturated solution (Figure 5-6). The RNT also exhibited stable luminescence intensity under long time at high temperatures as shown in Figure 5-7. These combined results imply the leakage of

the dyes from the RNT was negligible. If EuDT were to leak from the RNT, it would display attenuated intensity as EuDT was not stable in aqueous solution, particularly as the environment outside the polymer matrix.[3, 20, 29, 70] Observation of EuDT in aqueous condition (5% DMSO in Milli-Q water) verified that EuDT is unstable and exhibit a decay of luminescence intensity under long time observation (Figure 5-8). Therefore it is necessary to incorporate EuDT into a hydrophobic polymer, such as PS-MA, to improve its stability and quantum yield. In the case of rhodamine 800 leakages, the intensity ratio would fluctuate during the heating/ cooling cycles and would not show reversible response to the varying temperature. Nonetheless, rhodamine 800 leakage was not observed throughout any experiments (*in vitro* or *in vivo*) conducted using the EuDT–Rhodamine 800 RNT and the RNT displayed reversible response to the varying temperature.

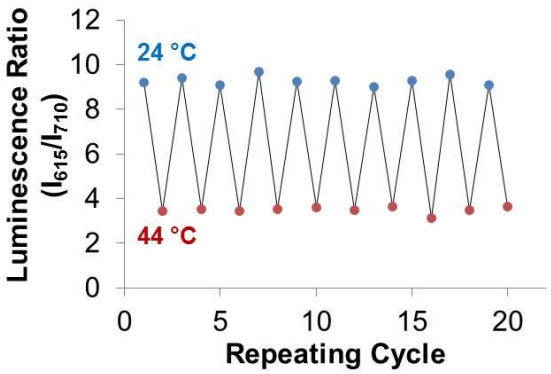

Figure 5-5: The reversibility of the RNT response against the heating-cooling cycle. The temperature was varied between 24 °C (blue circles) and 44 °C (red circles). For the EuDT channel, the excitation wavelength was 400 nm and the emission was recorded from 550 to 650 nm, while for the rhodamine 800 channel, the excitation wavelength was 635 nm and the emission was recorded from 660 to 750 nm. The luminescence ratio (I_{615}/I_{710}) was plotted against the number of heating-cooling cycle.

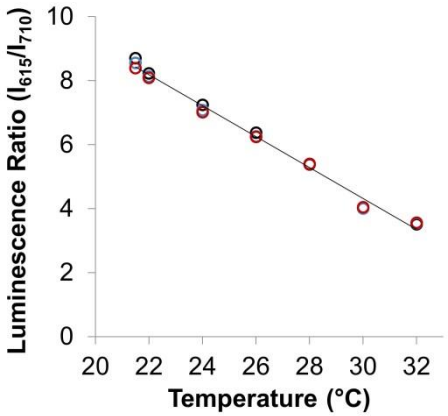

Figure 5-6: Reversibility of the luminescence ratio (I_{615}/I_{710}) of the RNT under N_2 saturated solution. (n = 3 trials, different colours represent independent trials)

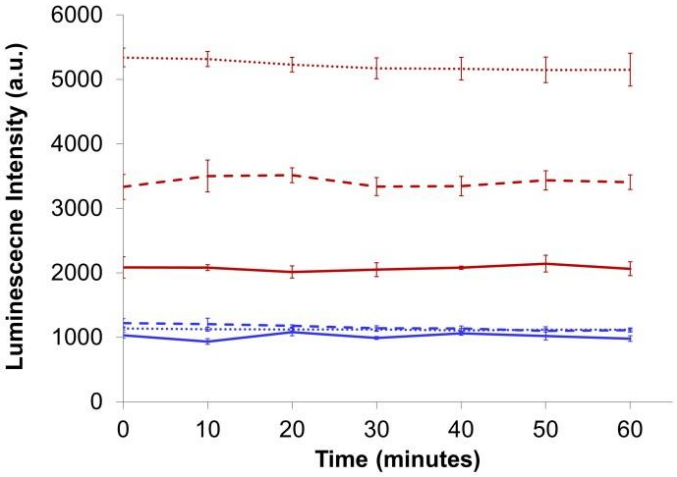

Figure 5-7: Stability of the RNT at higher temperatures for 60 minutes observation. Luminescence intensity of the RNT in PBS buffer recorded for EuDT (I_{615}) at 50 °C (red solid line), 40 °C (red dashed line), and 30 °C (red dotted line) as well as for Rhodamine 800 (I_{710}) at 50 °C (blue solid line), 40 °C (blue dashed line), and 30 °C (blue dotted line), plotted against time. The vertical bar represents the range of the intensities at different measurement trials (n = 3 trials). The insignificant variation in the intensities of EuDT and rhodamine 800 in the RNT recorded at high temperature indicates that both dyes were stable and did not leak out from the particles. If EuDT were to leak out, the intensity would drop as EuDT shows attenuated emission in aqueous solution (Figure 5-8). If rhodamine 800 were to leak out, the ratio value (I_{615}/ I_{710}) would fluctuate during the heating and cooling cycle and not reversibly respond to the varying temperature but throughout all the experiments, the ratio value was reversibly responded.

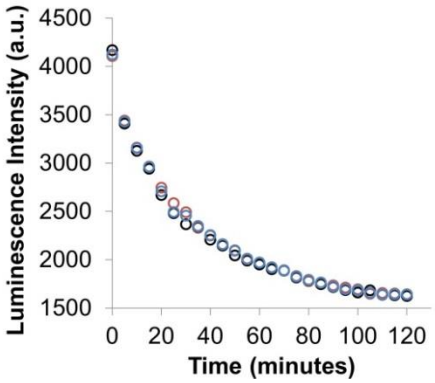

Figure 5-8: EuDT luminescence intensity decay in aqueous condition. Luminescence intensity of EuDT (I_{615}) under 5% DMSO in Milli-Q water was plotted against the measurement time (n = 3 trials, different colours represent independent trials).

5.2. RNT loading and *in vivo* RNT Calibration on *D. derbyana* Flight Muscle

The fabricated EuDT–Rhodamine 800 RNT was then demonstrated *in vivo* to monitor the temperature change in a small living animal, specifically to observe the heat production in the flight muscles of *D. derbyana* beetle as illustrated in Figure 2-9. The combination of EuDT and rhodamine 800 decreases the undesired signal from the autofluorescence of tissues, thus the luminescence intensity can be used directly for ratiometric analysis without the necessity to subtract the background. In order to load the RNT *in vivo* onto the dorsal longitudinal muscle (DLM), a major flight muscle of the beetle, a solution of the RNT in buffer was casted on top of the muscle and the RNTs were let to attach to the muscle surface. The luminescence intensity of the muscle in both EuDT and rhodamine 800 channels were measured before and after the RNT loading as shown in Figure 5-9. The autofluorescence was observed in both channels (EuDT and rhodamine 800, ‘before’ or blue histogram in Figure 5-9) which only account to 10-15 % of the luminescence intensity after the

RNT loading (red histogram in Figure 5-9). Moreover, the RNT was observed non-toxic for the beetle's muscular activity and overall survivorship as the RNT-loaded beetles were still alive and exhibited the pre-flight preparation, at least two days after the RNT was loaded (Figure 5-10).

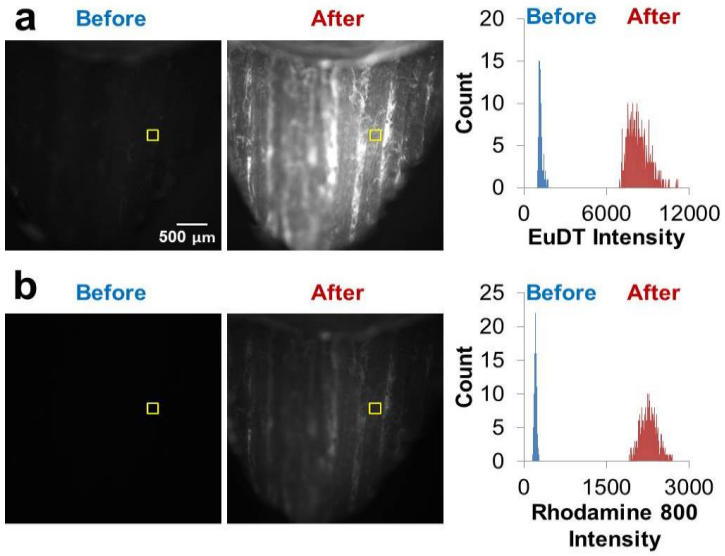

Figure 5-9: Luminescence intensity of flight muscle before and after loading of RNT. (a) EuDT channel and (b) Rhodamine 800 channel. The yellow rectangles indicate the ROI for intensity analysis shown in the histograms. The histograms on the right column show the luminescence intensity measured from the ROI depicted for before (blue bars) and after (red bars) RNT loading.

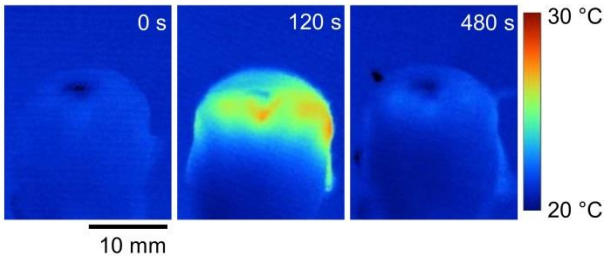

Figure 5-10: Infrared thermogram of beetle flight muscle during the pre-flight preparation, 2 days after RNT loading. The pre-flight preparation is still observed, even 2 days after application of the RNT on the flight muscles, indicating that the RNT has no toxicity.

After loading, the RNT were then tested for *in vivo* calibration on the flight muscle. The luminescence intensities of EuDT and rhodamine 800 were measured with

varying muscle temperature during external heating. The RNT-loaded muscle was subjected to a 980 nm laser (Figure 3-2) with increasing laser power to raise the muscle temperature as water molecules in the muscle absorbed the energy at 980 nm.[85] The muscle was then allowed to cool down naturally to room temperature at a reduced laser power. The temperature of the muscle was monitored by IRT throughout the heating-cooling process to ensure a uniform temperature along the examined muscle area (SD = ± 1°C).

The luminescence intensities of both EuDT (I_{615}) and rhodamine 800 (I_{710}) were measured by analysing the mean intensity within the multiple region of interest (ROIs), with a size of 68 µm x 68 µm each (Figure 5-11a). A minimum mean intensity value of 7000 (a.u.) measured from the EuDT channel was set to prevent failed RNT loading *in vivo*. The mean intensity ratio (I_{615}/I_{710}) from 24 ROIs was then plotted against temperature during the heating (from 20.7 °C to 28.4 °C, red dots in Figure 5-11b) and cooling (from 28.4 °C to 21.4 °C, red dots in Figure 5-11b) processes. The gradient of the plot during the heating process were then obtained as the temperature sensitivity of the RNT on the muscle with a value of –0.09 /°C. This value of absolute temperature sensitivity was much lower compared to the *in vitro* temperature sensitivity (–0.43 /°C) described earlier in section 5.1. It is commonly recognized that the absolute temperature sensitivity could be influenced by the different experimental setups owing to the fluctuation of luminescence intensity due to the difference in the excitation light source intensity and bandwidth, the sensor sensitivity, as well as the emission light bandwidth as discussed in section 4.2.. Thus, it is necessary to carry out calibration of the RNT

with different experimental setups.[12, 16] The absolute temperature sensitivity should be normalized to a certain I_{615}/I_{710} ratio at one temperature point (21.5 °C as in this study) in order to objectively compare the temperature sensitivity of the RNT measured by different setups. The normalized *in vivo* temperature sensitivity was –2.6 %/°C (Figure 5-12a), lower than such value measured *in vitro* (–4.0 %/°C, Figure 5-1d). Such normalized temperature sensitivity was also measured in another five different beetles and the values ranging between –1.6 %/°C to –2.6 %/°C (Figure 5-12b-f). It is also noted that the RNT also responded reversibly to the varying temperature during the heating-cooling (heating: red plots, cooling: blue plots in Figure 5-11 and Figure 5-12) cycles in the *in vivo* calibration performed in all the tested beetles, which suggest that photobleaching of whichever dyes was insignificant.

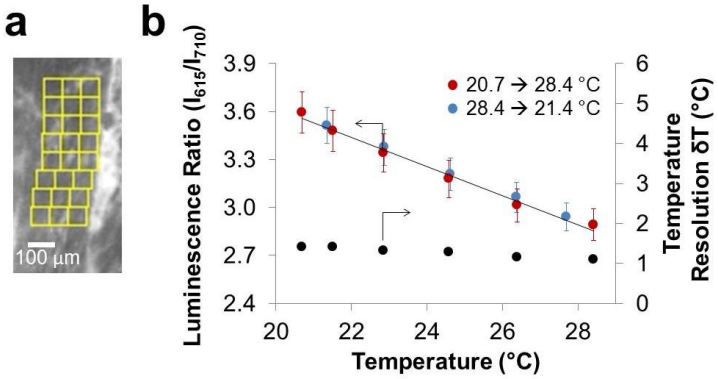

Figure 5-11: *In vivo* calibration of the RNT loaded onto the flight muscle of living *D. derbyana* beetle. The flight muscle was externally heated up and naturally cooled down. (a) Beetle flight muscle shown with 24 regions of interest (ROIs) for the ratiometric intensity analysis as in (b). The size of every ROI is 68 µm x 68 µm. (b) The mean luminescence intensity ratio (I_{615}/I_{710}) from the ROIs is plotted against varied temperatures. The ratio shifts during the heating (20.7 to 28.4 °C, red circles) and cooling (28.4 to 21.4 °C, blue circles) were plotted with the SD (vertical bars, n = 24 ROIs). The temperature sensitivity of RNT or the gradient of the curve, is –0.09 /°C (y = –0.09x + 5.4, R^2 = 0.99). The temperature resolution or δT, defined as SD divided by the temperature sensitivity (0.09 /°C), was plotted at every temperature as black circles.

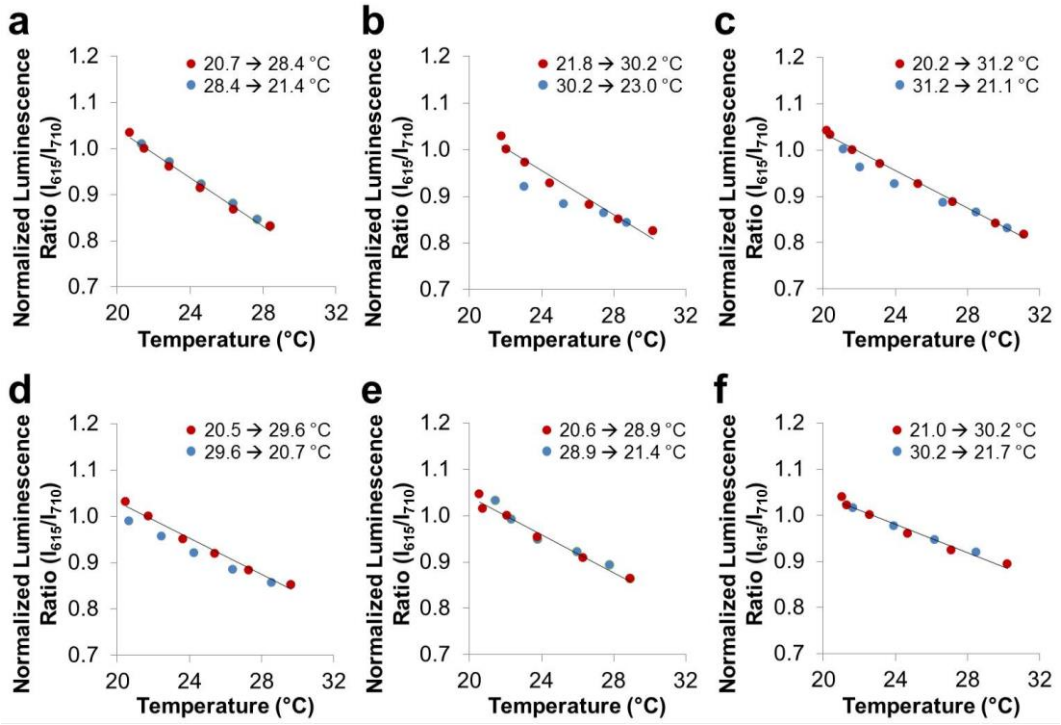

Figure 5-12: *In vivo* temperature sensitivity of the RNT on different beetles. The averaged *in vivo* normalized luminescence ratio (I_{615}/I_{710}, n = 24 ROIs) plotted against the varying temperature from flight muscles of different beetles during the heating (red circles) and cooling (blue circles). The relative temperature sensitivities, or the gradient of the normalized ratio value curves during heating, and the temperature by which the normalization was carried out were as follows: (a) –2.6 %/°C relative to 21.5 °C (y = –0.026x + 1.6, R^2 = 0.99); (b) –2.3 %/°C relative to 22.1 °C (y = –0.023x + 1.5, R^2 = 0.97); (c) –2.0 %/°C relative to 21.6 °C (y = –0.020x + 1.4, R^2 = 0.99); (d) –2.0 %/°C relative to 21.7 °C (y = –0.020x + 1.4, R^2 = 0.99); (e) –2.1 %/°C relative to 22.1 °C (y = –0.021x + 1.4, R^2 = 0.98); (f) –1.6 %/°C relative to 22.6 °C (y = –0.016x + 1.4, R^2 = 0.97).

For the purpose to quantify the accuracy of the measurement, the temperature resolution (δT) was calculated by taking the standard deviation (SD) of the measured intensity ratio (I_{615}/I_{710}) at each temperature divided by the overall absolute temperature sensitivity of the RNT (–0.09 /°C, Figure 5-11b).[5, 6, 12] The values of δT are between 1.0-1.4 °C throughout the examined temperature range (black plots in Figure 5-10), which is adequate to detect the temperature change due to the endogenous heat produced by the beetle during the pre-flight preparation.

5.3. *In vivo* Temperature Monitoring on *D. derbyana* Flight Muscle

The EuDT–Rhodamine 800 RNT-loaded beetle flight muscle was investigated to monitor the temperature shift owing to the endogenous heat produced by the beetle, in particular, during the pre-flight preparation. Pre-flight preparation in most insects is marked by a 'warm-up' activity through the simultaneous movement of the antagonist flight muscles, but no evident movement of the wings.[40-42] This activity could be provoked by a mechanical stimulation of a leg in which triggers the flight muscles to 'warm-up' and produce heat (Figure 5-13a, left & middle images). The beetle was then let to cool down and equilibrate with the room temperature naturally (Figure 5-13a, right image). The intensity ratio (I_{615}/I_{710}) was measured from the multiple ROIs (Figure 5-13b, left image) during the whole heating-cooling process while the large-scale overall muscle temperature was monitored by IRT. The I_{615}/I_{710} ratio measured at each ROI was then normalized by the ratio at 22.9 °C in order to fairly compare the ratio measured from the different ROIs as they displayed different absolute ratio values. The change of the normalized ratio value (ΔR) and the temperature shift (ΔT) measured by IRT are plotted versus time lapsed immediately after the pre-flight preparation was triggered. It was observed that the ΔR profiles follows the ΔT profile which suggests that the RNT can effectively detect the temperature shift owing to the endogenous heat production from the beetle's flight muscle during the pre-flight preparation.

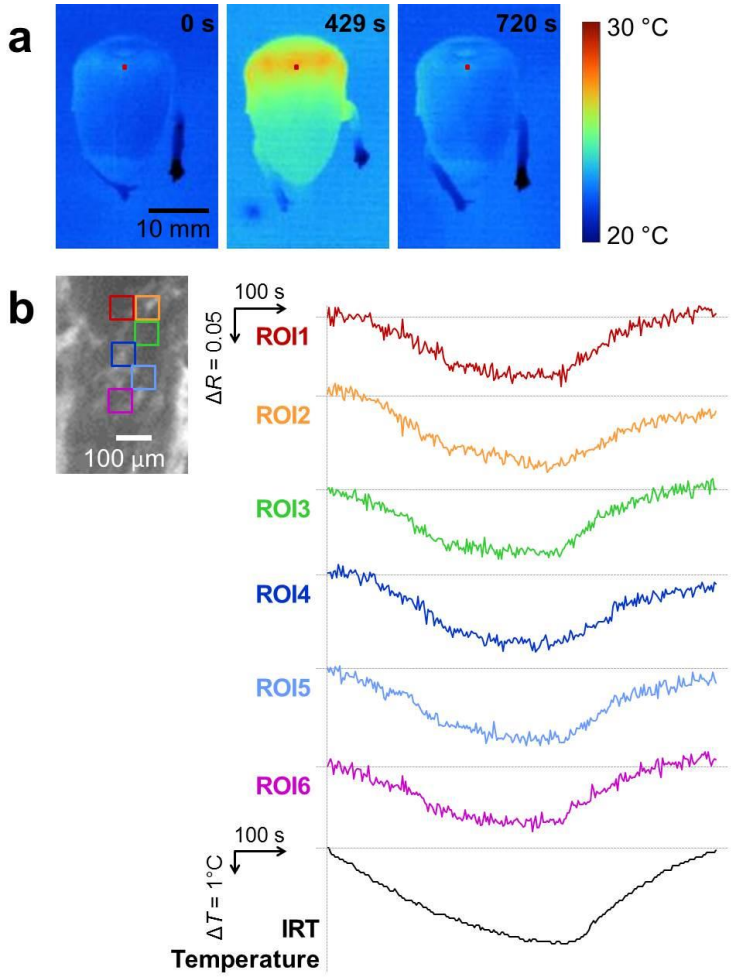

Figure 5-13: *In vivo* temperature monitoring and mapping of RNT loaded flight muscle of a living *D. derbyana* beetle. (a) IRT thermography showing the pre-flight preparation in which the muscle 'warm up'. The tiny red rectangles show the position and scale of the area of (b). (b) Temperature shifts detected by RNT loaded into the flight muscle at the different ROIs. The normalized ratio (I_{615}/I_{710}, relative to 22.9 °C) was plotted against the elapsed time after the initiation of the pre-flight preparation in the right panel. The size of every ROI is 68 µm x 68 µm. The temperature shifts measured by IRT (black line, from 22.5 °C to 26.7 °C and return back to 22.5°C) are plotted at the lowest trace.

From Figure 5-13, it could be inferred that each ROI displays a significantly different profiles of the normalized Δ*R*. For instance, ROI 5 displays a larger shift of the normalized intensity change (maximum Δ*R*) as compared to ROI 6, while such shifts are similar between ROIs 1 and 6. In order to unify the condition between the *in vivo* calibration and the pre-flight preparation, the shift in the

normalized intensity ratio (I_{615}/I_{710}), ΔR, was calculated as difference of the normalized intensity ratio between 22.9 °C and at 26.7 °C (as measured by IRT). *F*-test analysis verifies that the pre-flight preparation have larger variance of the normalized ΔR values amongst the 24 ROIs as compared to that values during the *in vivo* calibration (Figure 5-14). This suggests that the temperature shift is heterogeneous within the muscle fibre during the pre-flight preparation in contrast to the uniformly heated flight muscle during the calibration. This demonstration signifies that heat production or heat transfer occurs non-uniformly along a muscle fibre as measured by the RNT with a spatial resolution of 68 µm x 68 µm. Nonetheless, it is necessary to carry out further examination to expose more details of the heat transfer and heat production in the flight muscle of insects.

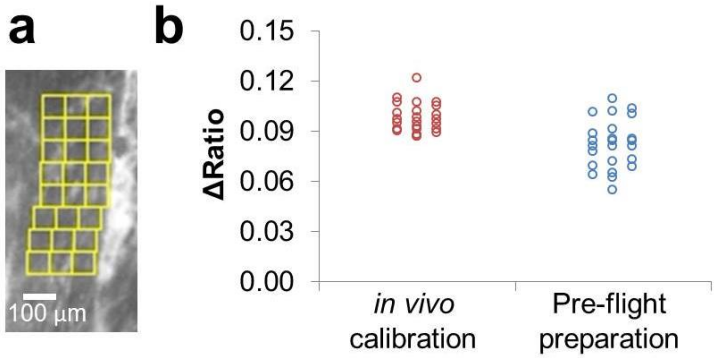

Figure 5-14: ΔR values variation during the *in vivo* calibration and the pre-flight preparation. The distribution of the normalized ΔR values, or the difference of the normalized intensity ratio, measured at 24 different ROIs under similar temperature change (ΔT, from 22.9 °C to 26.4 °C). The ratio at each temperature in both the *in vivo* calibration and the pre-flight preparation was normalized by the ratio at 22.9 °C (a) Locations of the 24 ROIs for analysis. (b) Distribution of the normalized ΔR values during the heating process of the *in vivo* calibration (red open circles) and the pre-flight preparation (blue open circles). The *F*-test showed that the *in vivo* calibration (mean ΔR = 0.098 ± 0.0085) and the pre-flight preparation (mean ΔR = 0.082 ± 0.0014) to have unequal variance ($F = 2.7534 > F_{0.025,\ 24,\ 24} = 2.0144$ at a 0.05 significance level) which suggests that the heat production and/or heat transfer significantly differ site-by-site in the pre-flight preparation as compared to the uniform heating in the *in vivo* calibration.

Chapter 6: Conclusion and Future Work

6.1. Conclusion

In this thesis, two types of intensity based ratiometric nanoparticle thermosensor (RNT) were prepared via the facile nano-precipitation method for temperature mapping in small animals, especially in *D. melanogaster* larvae and *D. derbyana* beetle. The whole preparation process was performed under a relatively low temperature and pressure with a fairly short time as compared to the other types of thermosensor preparation process. Ratiometric intensity analysis was utilized in order to cancel out the luminescence intensity variation due to the uneven particle distribution and dye concentration, the sample's surface topography, and the Z-axis displacement.

The first type of RNT comprise a combination of a temperature sensitive dye, EuDT and a less temperature sensitive dye, $Ir(ppy)_3$ as a reference for ratiometric analysis. Different polymer matrixes were investigated in order to optimize the size and emulsion stability of the RNT, and it is found that PS-MA and PMMA-MA could produce the stable RNTs with a size of 100–150 nm. The temperature sensitivity of these two RNTs was then examined *in vitro* by measuring their luminescence intensities at different temperatures. The PS-MA RNT shows the highest sensitivity of 0.039 /°C, while that of PMMA-MA RNT is 0.036 /°C. The temperature sensitivity of the PS-MA RNT was further verified by evaluating the emission of the dry particle substrate, and the value was 0.021 /°C with a temperature resolution less than 1 °C. The RNTs were then orally dosed to *D. melanogaster* larvae in order

to demonstrate the *in vivo* thermography with response to the change of the external temperature. The temperature sensitivity of the PS-MA RNT was 0.023 /°C and of the PMMA-MA RNT was 0.026 /°C, both lower compared to that of *in vitro* cuvette experiment results. Higher values of temperature resolution were observed for both RNTs in the *in vivo* observation of the RNTs dosed larvae (around 1.2 to 1.8 °C), which could give an indication of heterogeneous temperature distribution within the larvae.

The second type of RNT includes a combination of EuDT as the temperature sensitive dye and rhodamine 800 as the less-sensitive dye for reference. Owing to the specifically chosen and designed dyes combination, the contribution of autofluorescene as the background signal from the tissue can be reduced (to 10-15%), to allow direct ratiometric analysis using the intensity data without the necessity to subtract the background. The RNT displays high absolute temperature sensitivity *in vitro* of –0.43 /°C (–4.0 %/°C relative to 21.5 °C) and *in vivo* on beetle's flight muscle of –0.09 /°C (–2.6 %/°C relative to 21.5 °C, other test on 5 different beetles show values between –1.6 %/°C to –2.6 %/°C). The RNT exhibits the *in vivo* temperature resolution of 1.0-1.4 °C throughout the inspected temperature range between 20.7 to 28.4 °C with a spatial resolution defined by the ROI size of 68 µm x 68 µm. The RNT effectively detect the change in temperature at localized sites within the beetle's flight muscle, either during the external heat application in the calibration process or during the endogenous physiological heat production through the pre-flight preparation. Analysis of the change in the normalized intensity ratio (ΔR) suggests that the temperature shift at the localized

sites is heterogeneous during the pre-flight preparation in contrary to the uniform heating during the *in vivo* calibration. This finding proposes that heat production or heat transfer may occur non-uniformly within a muscle fibre as observed by the RNT. The demonstration of the RNT system for *in vivo* thermography in small living animals could serves a potential technology for high spatial resolution temperature detection, particularly to investigate various heat production and heat transfer activities at the microscopic level, in small living animals.

This project has shown the potential use of luminescence RNT as a powerful sensor for micro thermography in small animals as compared to conventional thermosensors. The facile and simple preparation process provides the advantage for tuning the particle size and properties to optimize the performance of the RNT with a relatively simple process and short fabrication time. Moreover, the RNT also offer a possibility to map out the temperature distribution with high spatial and temperature resolution within the animals which could stimulate a better understanding of thermogenesis through endothermic physiological heat production at the different local sites.

6.2. Future Work

The prepared RNTs: EuDT–$Ir(ppy)_3$ RNT and EuDT–Rhodamine 800 RNT succeeded in visualizing the micro-scale temperature distribution within small living animals, such as: *D. melanogaster* larvae and *D. derbyana* beetle. However, the RNT itself is still not able to precisely measure the exact temperature at the

various local sites. Rather, the RNT works by detecting the temperature shift utilizing the change in the measured ratio value. Accurate temperature information at such small scale is necessary to comprehend a better interpretation of thermogenesis in small animals. The following issues are necessary to be addressed in future studies:

1. Autofluorescence interference of tissues in the short wavelength, especially in the $Ir(ppy)_3$ channel. Autofluorescence could cause over- or under-estimation of the luminescence ratio value because the individual intensity value of $Ir(ppy)_3$ is escalated. As RIM analysis is unable to overcome the problem of autofluorescence, it is necessary to substitute the reference dye, $Ir(ppy)_3$, with another dye that excitable at the visible wavelength range (to reduce phototoxicity of the dye) and displays emission at a long wavelength area (Infrared emission) far off the autofluorescence range, for example by using rhodamine 800 as described in chapter 5. Alternatively, the true intensity value could be corrected by background subtraction.[7]
2. RNT design of the dyes selection. Although the use of rhodamine 800 as a reference dye could reduce the undesired contribution from autofluorescence as described in point (1) above owing to its long wavelength excitation and emission, rhodamine 800 could not be excited simultaneously with EuDT due to their different excitation wavelengths. Using the combination of EuDT and rhodamine 800, it is required to have a two-excitation wavelength light source to allow for ratiometric measurement. Enhancement could be made by selectively picking the temperature sensitive dye and the less

temperature sensitive dye pair to have a single wavelength or a narrow range of wavelengths for excitation while keeping two distinct emissions.

3. Improvement of the temperature resolution (δT) of the RNT. δT could be boosted by optimizing the polymer and dyes combination to obtain RNT with higher temperature sensitivity as the δT of the RNT is calculated by dividing the SD with the temperature sensitivity. Improvement of δT implies that the measurement results is more reliable with low deviation.
4. Application of the RNT to detect the intrinsic physiological heat produced in different study animals. In the observation in *D. melanogaster* larvae using the EuDT–$Ir(ppy)_3$, temperature change was externally induced using a microwarm plate which would not reflect the internal heat generated. Examination of the intrinsic heat production in animals could give a better understanding for thermogenesis study. One particular example is the examination of the endogenous heat production during the pre-flight preparation in *D. derbyana* beetle using the EuDT–Rhodamine 800 as described in chapter 5. An interesting research application would be to apply the RNT to measure the heat production in *D. melanogaster* fly.
5. Perform the RNT calibration on the organelle / tissue of interest. As described earlier, the sensitivity of the RNT could vary with different setup and sample. Thus, RNT calibration performed with the same setup and sample is crucial to gather a more accurate data and a reliable interpretation of the results.

6. Designing the RNT with additional function. The RNT preparation process via the nano-precipitation method allows doping of additional functional moiety. For instance, one can embed iron oxide into the RNT to create supermagnetic RNT which enables the control of the RNT's position by utilizing magnetic field.[89] Alternatively, it is also possible to embed other chemical indicators to the RNT, for example to measure the calcium burst coupled with temperature during the pre-flight preparation in muscle.[90]

References

1. P. R. Childs (2001) Practical temperature measurement. Butterworth-Heinemann.
2. C. D. S. Brites, P. P. Lima, N. J. O. Silva, A. Millan, V. S. Amaral, et al. "Thermometry at the nanoscale", *Nanoscale* 4: pp.4799-4829.
3. X. Wang, O. S. Wolfbeis, R. J. Meier "Luminescent probes and sensors for temperature", *Chem Soc Rev* 42: pp.7834-7869.
4. C. Wang, R. Xu, W. Tian, X. Jiang, Z. Cui, et al. "Determining intracellular temperature at single-cell level by a novel thermocouple method", *Cell Res* 21: pp.1517.
5. C. Gota, K. Okabe, T. Funatsu, Y. Harada, S. Uchiyama "Hydrophilic fluorescent nanogel thermometer for intracellular thermometry", *J Am Chem Soc* 131: pp.2766-2767.
6. K. Okabe, N. Inada, C. Gota, Y. Harada, T. Funatsu, et al. "Intracellular temperature mapping with a fluorescent polymeric thermometer and fluorescence lifetime imaging microscopy", *Nat Commun* 3: pp.705.
7. K. Gonda, M. Miyashita, H. Higuchi, H. Tada, T. M. Watanabe, et al. "Predictive diagnosis of the risk of breast cancer recurrence after surgery by single-particle quantum dot imaging", *Sci Rep* 5: pp.14322.
8. J. B. Weaver "Bioimaging: Hot nanoparticles light up cancer", *Nat Nanotechnol* 5: pp.630-631.
9. B. Lahiri, S. Bagavathiappan, T. Jayakumar, J. Philip "Medical applications of infrared thermography: a review", *Infrared Phys Techn* 55: pp.221-235.
10. J. Christofferson, K. Maize, Y. Ezzahri, J. Shabani, X. Wang, et al. "Microscale and Nanoscale Thermal Characterization Techniques", *J Electron Packaging* 130: pp.041101-041101.
11. M. Asheghi, Y. Yang (2005) Micro-and nano-scale diagnostic techniques for thermometry and thermal imaging of microelectronic and data storage devices. Microscale Diagnostic Techniques. Springer. pp. 155-196.

12. S. Arai, Ferdinandus, S. Takeoka, S. Ishiwata, H. Sato, et al. "Micro-thermography in millimeter-scale animals by using orally-dosed fluorescent nanoparticle thermosensors", *Analyst* 140: pp.7534-7539.
13. G. R. Bright, G. W. Fisher, J. Rogowska, D. L. Taylor "Fluorescence ratio imaging microscopy: temporal and spatial measurements of cytoplasmic pH", *J Cell Biol* 104: pp.1019-1033.
14. K. Oyama, M. Takabayashi, Y. Takei, S. Arai, S. Takeoka, et al. "Walking nanothermometers: spatiotemporal temperature measurement of transported acidic organelles in single living cells", *Lab Chip* 12: pp.1591-1593.
15. H. Peng, S. H. Huang, O. S. Wolfbeis "Ratiometric fluorescent nanoparticles for sensing temperature", *J Nanopart Res* 12: pp.2729-2733.
16. Y. Takei, S. Arai, A. Murata, M. Takabayashi, K. Oyama, et al. "A Nanoparticle-Based Ratiometric and Self-Calibrated Fluorescent Thermometer for Single Living Cells", *ACS Nano* 8: pp.198-206.
17. X. Wang, X. Song, C. He, C. J. Yang, G. Chen, et al. "Preparation of Reversible Colorimetric Temperature Nanosensors and Their Application in Quantitative Two-Dimensional Thermo-Imaging", *Anal Chem* 83: pp.2434-2437.
18. M. Homma, Y. Takei, A. Murata, T. Inoue, S. Takeoka "A ratiometric fluorescent molecular probe for visualization of mitochondrial temperature in living cells", *Chem Commun* 51: pp.6194-6197.
19. J. R. Lakowicz, H. Szmacinski, K. Nowaczyk, K. W. Berndt, M. Johnson "Fluorescence lifetime imaging", *Anal Biochem* 202: pp.316-330.
20. B. B. J. Basu, N. Vasantharajan "Temperature dependence of the luminescence lifetime of a europium complex immobilized in different polymer matrices", *J Lumin* 128: pp.1701-1708.
21. M. T. Berry, P. S. May, H. Xu "Temperature Dependence of the Eu3+ 5D0 Lifetime in Europium Tris(2,2,6,6-tetramethyl-3,5-heptanedionato)", *J Phys Chem* 100: pp.9216-9222.
22. E. M. Graham, K. Iwai, S. Uchiyama, A. P. de Silva, S. W. Magennis, et al. "Quantitative mapping of aqueous microfluidic temperature with sub-degree

resolution using fluorescence lifetime imaging microscopy", *Lab Chip* 10: pp.1267-1273.

23. A. Jablonski "On the notion of emission anisotropy", *Bull Acad Polon Sci, Ser sci math astr phys* 8: pp.259-264.
24. J. S. Donner, S. A. Thompson, C. Alonso-Ortega, J. Morales, L. G. Rico, et al. "Imaging of Plasmonic Heating in a Living Organism", *ACS Nano* 7: pp.8666-8672.
25. S. Kiyonaka, T. Kajimoto, R. Sakaguchi, D. Shinmi, M. Omatsu-Kanbe, et al. "Genetically encoded fluorescent thermosensors visualize subcellular thermoregulation in living cells", *Nat Methods* 10: pp.1232-1238.
26. J. Llopis, J. M. McCaffery, A. Miyawaki, M. G. Farquhar, R. Y. Tsien "Measurement of cytosolic, mitochondrial, and Golgi pH in single living cells with green fluorescent proteins", *Proc Natl Acad Sci USA* 95: pp.6803-6808.
27. J. R. Lakowicz (2013) Principles of fluorescence spectroscopy. Springer Science & Business Media.
28. Ferdinandus, S. Arai, S. Ishiwata, M. Suzuki, H. Sato (2015) Self-calibrated fluorescent thermometer nanoparticles enable *in vivo* micro thermography in milimeter scale living animals. Solid-State Sensors, Actuators and Microsystems (TRANSDUCERS), 2015 Transducers - 2015 18th International Conference on. pp. 2228-2231.
29. M. D. McGehee, T. Bergstedt, C. Zhang, A. P. Saab, M. B. O'Regan, et al. "Narrow bandwidth luminescence from blends with energy transfer from semiconducting conjugated polymers to europium complexes", *Adv Mater* 11: pp.1349-1354.
30. M. Mitsuishi, S. Kikuchi, T. Miyashita, Y. Amao "Characterization of an ultrathin polymer optode and its application to temperature sensors based on luminescent europium complexes", *J Mater Chem* 13: pp.2875-2879.
31. C. Chapman, Y. Liu, G. Sonek, B. Tromberg "The use of exogenous fluorescent probes for temperature measurements in single living cells", *Photochem Photobiol* 62: pp.416-425.

32. J. S. Donner, S. A. Thompson, M. P. Kreuzer, G. Baffou, R. Quidant "Mapping Intracellular Temperature Using Green Fluorescent Protein", *Nano Lett* 12: pp.2107-2111.
33. J. M. Yang, H. Yang, L. Lin "Quantum Dot Nano Thermometers Reveal Heterogeneous Local Thermogenesis in Living Cells", *ACS Nano* 5: pp.5067-5071.
34. S. Arai, M. Suzuki, S. J. Park, J. S. Yoo, L. Wang, et al. "Mitochondria-targeted fluorescent thermometer monitors intracellular temperature gradient", *Chem Commun* 51: pp.8044-8047.
35. S. Arai, S. C. Lee, D. Zhai, M. Suzuki, Y. T. Chang "A Molecular Fluorescent Probe for Targeted Visualization of Temperature at the Endoplasmic Reticulum", *Sci Rep* 4: pp.6701.
36. L. M. Houdebine "The methods to generate transgenic animals and to control transgene expression", *J Biotechnol* 98: pp.145-160.
37. Ferdinandus, S. Arai, S. Ishiwata, M. Suzuki, H. Sato "Oral Dosing of Chemical Indicators for *in vivo* Monitoring of Ca^{2+} Dynamics in Insect Muscle", *PLoS ONE* 10.
38. M. L. May "Insect thermoregulation", *Annu Rev Entomol* 24: pp.313-349.
39. H. Esch "Body temperature and flight performance of honey bees in a servo-mechanically controlled wind tunnel", *J Comp Psychol* 109: pp.265-277.
40. A. Krogh, E. Zeuthen "The Mechanism of Flight Preparation in Some Insects", *J Exp Biol* 18: pp.1-10.
41. T. M. Casey, J. R. Hegel, C. S. Buser "Physiology and energetics of pre-flight warm-up in the eastern tent caterpillar moth *Malacosoma americanum*", *J Exp Biol* 94: pp.119-135.
42. B. A. Block "Thermogenesis in muscle", *Annu Rev Physiol* 56: pp.535-577.
43. D. Leston, J. Pringle, D. White "Muscular activity during preparation for flight in a beetle", *J Exp Biol* 42: pp.409-414.
44. G. A. Bartholomew, T. M. Casey "Body temperature and oxygen consumption during rest and activity in relation to body size in some tropical beetles", *J Therm Biol* 2: pp.173-176.

45. G. A. Bartholomew, T. M. Casey "Oxygen Consumption of Moths During Rest, Pre-Flight Warm-Up, and Flight In Relation to Body Size and Wing Morphology", *J Exp Biol* 76: pp.11-25.
46. R. K. Josephson "Contraction Kinetics of the Fast Muscles used in Singing by a Katydid", *J Exp Biol* 59: pp.781-801.
47. F. Seebacher, C. Franklin "Physiological mechanisms of thermoregulation in reptiles: a review", *J Comp Physiol B* 175: pp.533-541.
48. J. E. P. W. Bicudo, C. R. Vianna, J. G. Chaui-Berlinck "Thermogenesis in Birds", *Biosci Rep* 21: pp.181-188.
49. J. Speakman, S. Ward "Infrared thermography: principles and applications", *Zoology-Jena*- 101: pp.224-232.
50. M. Carosena, M. C. Giovanni "Recent advances in the use of infrared thermography", *Meas Sci Technol* 15: pp.R27.
51. K. T. Grattan, Z. Y. Zhang (1995) Fiber optic fluorescence thermometry. Springer Science & Business Media.
52. S. Modi, M. Swetha, D. Goswami, G. D. Gupta, S. Mayor, et al. "A DNA nanomachine that maps spatial and temporal pH changes inside living cells", *Nat Nanotechnol* 4: pp.325-330.
53. K. Buckler, R. Vaughan-Jones "Application of a new pH-sensitive fluoroprobe (carboxy-SNARF-1) for intracellular pH measurement in small, isolated cells", *Pflügers Archiv* 417: pp.234-239.
54. K. Ohtsuka, S. Sato, Y. Sato, K. Sota, S. Ohzawa, et al. "Fluorescence imaging of potassium ions in living cells using a fluorescent probe based on a thrombin binding aptamer–peptide conjugate", *Chem Commun* 48: pp.4740-4742.
55. M. K. Kuimova, S. W. Botchway, A. W. Parker, M. Balaz, H. A. Collins, et al. "Imaging intracellular viscosity of a single cell during photoinduced cell death", *Nat Chem* 1: pp.69-73.
56. L. Wang, Y. Xiao, W. Tian, L. Deng "Activatable rotor for quantifying lysosomal viscosity in living cells", *J Am Chem Soc* 135: pp.2903-2906.
57. S. Li, K. Zhang, J.-M. Yang, L. Lin, H. Yang "Single quantum dots as local temperature markers", *Nano Lett* 7: pp.3102-3105.

58. P. Löw, B. Kim, N. Takama, C. Bergaud "High-Spatial-Resolution Surface-Temperature Mapping Using Fluorescent Thermometry", *Small* 4: pp.908-914.
59. G. Baffou, C. Girard, R. Quidant "Mapping heat origin in plasmonic structures", *Phys Rev Lett* 104: pp.136805.
60. L. Goss, A. Smith, M. Post "Surface thermometry by laser-induced fluorescence", *Rev Sci Instrum* 60: pp.3702-3706.
61. N. Ishiwada, T. Ueda, T. Yokomori "Characteristics of rare earth (RE= Eu, Tb, Tm)-doped Y_2O_3 phosphors for thermometry", *Luminescence* 26: pp.381-389.
62. E. J. McLaurin, L. R. Bradshaw, D. R. Gamelin "Dual-emitting nanoscale temperature sensors", *Chem Mater* 25: pp.1283-1292.
63. T. Fukatsu, K. Watanabe, Y. Sekiguchi "Specific detection of intracellular symbiotic bacteria of aphids by oligonucleotide-probed in situ hybridization", *Appl Entomol Zool* 33: pp.461-472.
64. R. Koga, T. Tsuchida, T. Fukatsu "Quenching autofluorescence of insect tissues for *in situ* detection of endosymbionts", *Appl Entomol Zool* 44: pp.281-291.
65. T. Thimm, C. C. Tebbe "Protocol for rapid fluorescence in situ hybridization of bacteria in cryosections of microarthropods", *Appl Environ Microbiol* 69: pp.2875-2878.
66. A. V. Klaus, V. L. Kulasekera, V. Schawaroch "Three-dimensional visualization of insect morphology using confocal laser scanning microscopy", *J Microsc* 212: pp.107-121.
67. J. L. Pittman, C. S. Henry, S. D. Gilman "Experimental studies of electroosmotic flow dynamics in microfabricated devices during current monitoring experiments", *Anal Chem* 75: pp.361-370.
68. T. Glawdel, Z. Almutairi, S. Wang, C. Ren "Photobleaching absorbed Rhodamine B to improve temperature measurements in PDMS microchannels", *Lab Chip* 9: pp.171-174.
69. H. F. Arata, P. Löw, K. Ishizuka, C. Bergaud, B. Kim, et al. "Temperature distribution measurement on microfabricated thermodevice for single biomolecular observation using fluorescent dye", *Sensor Actuat B Chem* 117: pp.339-345.

70. G. E. Khalil, K. Lau, G. D. Phelan, B. Carlson, M. Gouterman, et al. "Europium beta-diketonate temperature sensors: Effects of ligands, matrix, and concentration", *Rev Sci Instrum* 75: pp.192-206.
71. H. Peng, M. I. Stich, J. Yu, L. n. Sun, L. H. Fischer, et al. "Luminescent europium (III) nanoparticles for sensing and imaging of temperature in the physiological range", *Adv Mater* 22: pp.716-719.
72. C. D. S. Brites, P. P. Lima, N. J. O. Silva, A. Millán, V. S. Amaral, et al. "Thermometry at the nanoscale using lanthanide-containing organic–inorganic hybrid materials", *J Lumin* 133: pp.230-232.
73. L. D. Carlos, R. A. Ferreira, V. d. Z. Bermudez, S. J. Ribeiro "Lanthanide-Containing Light-Emitting Organic–Inorganic Hybrids: A Bet on the Future", *Adv Mater* 21: pp.509-534.
74. H. G. Schild "Poly (N-isopropylacrylamide): experiment, theory and application", *Prog Polym Sci* 17: pp.163-249.
75. C. Pietsch, U. S. Schubert, R. Hoogenboom "Aqueous polymeric sensors based on temperature-induced polymer phase transitions and solvatochromic dyes", *Chem Commun* 47: pp.8750-8765.
76. C. Vauthier, K. Bouchemal "Methods for the preparation and manufacture of polymeric nanoparticles", *Pharm Res* 26: pp.1025-1058.
77. B. Nagavarma, H. K. Yadav, A. Ayaz, L. Vasudha, H. Shivakumar "Different techniques for preparation of polymeric nanoparticles—a review", *Asian J Pharm Clin Res* 5: pp.16-23.
78. U. Bilati, E. Allémann, E. Doelker "Development of a nanoprecipitation method intended for the entrapment of hydrophilic drugs into nanoparticles", *European Journal of Pharmaceutical Sciences* 24: pp.67-75.
79. M. Bhaumik "Quenching and Temperature Dependence of Fluorescence in Rare-Earth Chelates", *J Chem Phys* 40: pp.3711-3715.
80. S. Weissman "Intramolecular energy transfer the fluorescence of complexes of europium", *J Chem Phys* 10: pp.214-217.

81. K. Goushi, Y. Kawamura, H. Sasabe, C. Adachi "Unusual phosphorescence characteristics of Ir (ppy) 3 in a solid matrix at low temperatures", *Jpn J Appl Phys* 43: pp.L937.
82. T. Tsuboi, N. Aljaroudi "Phosphorescence Decay Process of $Ir(ppy)_3$: Temperature Dependence of Decay Time", *Jpn J Appl Phys* 44: pp.591.
83. A. Alessi, M. Salvalaggio, G. Ruzzon "Rhodamine 800 as reference substance for fluorescence quantum yield measurements in deep red emission range", *J Lumin* 134: pp.385-389.
84. H. Sato, C. W. Berry, Y. Peeri, E. Baghoomian, B. E. Casey, et al. "Remote radio control of insect flight", *Front Integr Neurosci* 3: pp.24.
85. R. J. McNichols, A. Gowda, M. Kangasniemi, J. A. Bankson, R. E. Price, et al. "MR thermometry-based feedback control of laser interstitial thermal therapy at 980 nm", *Lasers Surg Med* 34: pp.48-55.
86. R. F. Chapman (1998) The insects: structure and function. Cambridge university press.
87. D. Ozkaya, W. Zhou, J. M. Thomas, P. Midgley, V. J. Keast, et al. "High-resolution imaging of nanoparticle bimetallic catalysts supported on mesoporous silica", *Catal Lett* 60: pp.113-120.
88. P. A. Midgley, M. Weyland, J. M. Thomas, B. F. Johnson "Z-Contrast tomography: a technique in three-dimensional nanostructural analysis based on Rutherford scattering", *Chem Commun*: pp.907-908.
89. S. H. Im, T. Herricks, Y. T. Lee, Y. Xia "Synthesis and characterization of monodisperse silica colloids loaded with superparamagnetic iron oxide nanoparticles", *Chem Phys Lett* 401: pp.19-23.
90. H. Itoh, S. Arai, T. Sudhaharan, S.-C. Lee, Y.-T. Chang, et al. "Direct organelle thermometry with fluorescence lifetime imaging microscopy in single myotubes", *Chem Commun* 52: pp.4458-4461.